

Hyper-Kamiokande Outer Detector Light Injector System Technical Note

Balint Bogdan*, Sam Jenkins, Steve Boyd, Keith Jewkes, Menai Lamers James,
Grace Hannaford, Ankush Mitra

September 25, 2025

5 Contents

6	0 Version history	3
7	1 Introduction	4
8	2 Light Injection System Overview and Requirements	4
9	3 OD PMT Saturation Study	5
10	3.1 Light Injector Simulation	5
11	3.2 Diffuser and OD Parameters	7
12	3.3 Saturation Study	7
13	3.4 Results	9
14	4 Diffuser Design	10
15	4.1 ID Diffuser Hemisphere Design	10
16	4.1.1 Inner Detector Diffuser Design	10
17	4.1.2 Diffuser Profile Measurement System	10
18	4.1.3 Diffuser Power Measurement System	12
19	4.2 OD Diffuser Design	14
20	5 OD Diffuser Mounting System and Installation	15
21	6 Pulser Board	16
22	6.1 Pulser Board Overview	16
23	6.2 Physical dimensions and construction	16
24	6.3 LED	19
25	6.3.1 Overview	19
26	6.3.2 Switching Circuit	19
27	6.3.3 Switch Selection	19
28	6.3.4 Testing	20
29	6.4 LVDS to TTL Converter	23
30	6.5 Power Supplies	24
31	6.6 Connector	25
32	6.7 Fibre Coupler	27

*bbogdan@liverpool.ac.uk

33	6.8 Photon Yield Tests	28
34	6.9 Production	28
35	6.10 Changes Expected from v0.9 to v1.0	28
36	6.10.1 LED and Switching Circuit	28
37	6.10.2 LVDS-to-TTL converter	28
38	6.10.3 Power supplies	28
39	6.10.4 Connector	29
40	6.10.5 Fibre coupler	29
41	7 Server Rack and Cooling	29
42	8 LED Monitoring	30
43	9 Control System for LEDs	30
44	10 Crate Electronics	31
45	10.1 Overview	31
46	10.2 Blade	31
47	10.3 Backplane	32
48	10.4 Eurocard	33
49	11 Conclusions	34

50 **0 Version history**

- 51 • v0.99 - First release by Balint circulated to Liverpool group for internal review
- 52 • v1 - [Sam]: Ported over to github for continued development, as we hit compilation
53 time on overleaf. Initial pass through to fix wording and rewrite some sections. Also
54 integrating Warwick TN on OD diffuser, and Liz's work on the OD saturation studies.
55 Some reordering of structure to make it flow better.

56 **1 Introduction**

57 Hyper-Kamiokande is a large scale water Cherenkov detector with two main sections, an
58 inner detector (ID) and an outer detector (OD). The OD volume of Hyper-K is a one meter
59 wide annular ring on the circumference of the detector. This space is designed to tag charged
60 particles, such as cosmic ray muons or particles from interactions in the surrounding rock,
61 entering the detector. In addition, the OD volume will be used as working space for instal-
62 lation activities. Once complete, it will be optically separated from the ID volume, and will
63 be instrumented with 3,600 outward facing 8 cm photomultipliers tubes (PMTs). These will
64 each surrounded by wavelength shifting (WLS) plates to increase photocoverage.

65 In order to achieve the precision measurements Hyper-K aims to make, precise calibration
66 of the detector is required. For the OD, a light injection (LI) system will be employed,
67 allowing for known quantities of light to be injected into the detector region. This will
68 consist of 122 diffusers and 12 collimators. The diffuser system, which is described in this
69 technical note, will be used to measure gain and timing properties of the OD PMTs, and
70 will be powered by dedicated pulsed LED sources. The 12 OD collimators are identical to
71 those uses in the ID system, and will be integrated into the ID laser system. Full details on
72 that system, along with investigations of the fibre optics that will be employed for the OD
73 system, can be found in [1].

74 **2 Light Injection System Overview and Requirements**

75 The OD diffuser system will be composed of 122 bare diffusers, installed on the outward
76 facing side of the PMT support structure. The diffuser design is discussed in Section 4.
77 These will each be illuminated by individual LED pulser boards, with 365 nm LEDs. This
78 will require at least 122 dedicated LED pulsers, and spares should be readily available for hot-
79 swapping should a board encounter issues. Full details of the pulser board design are given
80 in Section 6. The pulser boards will be powered and controlled by commercially-available
81 Field Programmable Grid Array (FPGA) boards. The control system architecture for these
82 consists of three primary components:

- 83 • **Blade:** Interfaces directly with the FPGA, distributing all differential signals into the
84 crate system.
- 85 • **Backplane:** Routes differential signals to the pulser boards and provides the primary
86 power distribution, accepting 12 V and ± 5 V inputs.
- 87 • **Eurocards:** Host the pulser boards, receive power and differential signals from the
88 backplane, and incorporate the necessary circuitry for laser triggering.

89 Further details on the control system and individual electronics crate components are given
90 in Sections 9 and 10 respectively.

91 Light will be transported between the pulsers and diffusers by a series of fibre optic
92 cables; following the investigations in [1] the Thorlabs FP400URT [2] is targeted for this.
93 Due to production limitations, it is not possible to keep all fibre path lengths the same.
94 Instead there will be five different lengths: 50 m, 80 m, 106 m, 124 m and 168 m. The
95 light output after signal attenuation and dispersion in these fibres should be as consistent
96 as possible, which will require fine tuning given the different amounts of attenuation and
97 dispersion which pulses will experience based on fibre length.

98 The initial design requirements for the system are to produce pulse widths out of the
99 diffuser of between 1–10 ns, with a photon yield in the range 1–15 million photons per pulse
100 (ppp). The 10 ns limit is driven by the timing resolution of the WLS plates. The photon

101 yield target here is more of a goal than a requirement, and saturation studies were performed
102 using numbers motivated by system performance. These are summarised in Section 3.

103 The below paragraph should split up. The first half has been rewritten into the above
104 paragraph, the second should be fleshed out for the photon yield test section.

105 Pulse width should ideally be between 1-10 ns and the photon count from 1-15 million
106 photons, but higher limits are preferable. The lower limits are not possible to achieve, as
107 the fibre dispersion will create a minimum pulse width, which is 4.5 ns at 180 metres, and
108 if we try to achieve large light output it will compromise our lower light output, so we can
109 only achieve around 100,000 photons per pulse at minimum. While these compromises are not
110 ideal, the fibre selection limits our capabilities on hitting the required theoretical targets.

111 3 OD PMT Saturation Study

112 The light injection system in the OD will use collimated and diffuse light injection to calibrate
113 the PMTs and to measure the optical properties (scattering and attenuation) of water, as
114 well as any degradation in Tyvek reflectivity over the course of operation.

115 Diffuse light sources will be used for in-situ calibration of the PMT charge response.
116 Light will be injected at very low levels to measure the single-photoelectron charge response,
117 and the requirement to achieve single-photoelectron coverage across all PMTs was used to
118 determine the number of light injectors required for the light injection calibration system, as
119 reported in the Outer Detector Technical Report [3]. In order to calibrate the PMTs across
120 their entire range, the light injection system must also be capable of illuminating PMTs to
121 saturation, to understand the change in their response as they approach saturation.

122 This section describes the use of diffuse light injection to evaluate the suitability of light
123 sources for in-situ measurements of the PMT saturation response. Section 3.1 describes the
124 diffuser simulation, Section 3.2 gives details of the OD geometry and diffuser parameters
125 used, and Sections 3.3 and 3.4 describe the scope, analysis and results of the saturation
126 study.

127 3.1 Light Injector Simulation

128 The planned light injection calibration system will consist of 122 sources, as determined by
129 maximising the single-photoelectron coverage of all of the OD PMTs [3]. The division of
130 sources between the endcaps and barrels, and their positions in terms of the overall geometry,
131 has been altered since [3], following an update of the design and geometry in the simulation.
132 Figure 1 shows the updated diffuse light injector (LI) with respect to OD PMT positions.
133 The diffusers have been positioned as close to equidistant as possible from the surrounding
134 PMTs, next to a strut in an empty cell.

135 A new LI generator has been written within the framework of WCSim [4]. This allows
136 the user to define the characteristics of the LI within a data file input to the simulation. The
137 following characteristics can be defined:

- 138 • Global position within the detector geometry,
- 139 • Direction of the LI axis,
- 140 • Wavelength of the optical photons
- 141 • Pulse width
- 142 • Photons per pulse

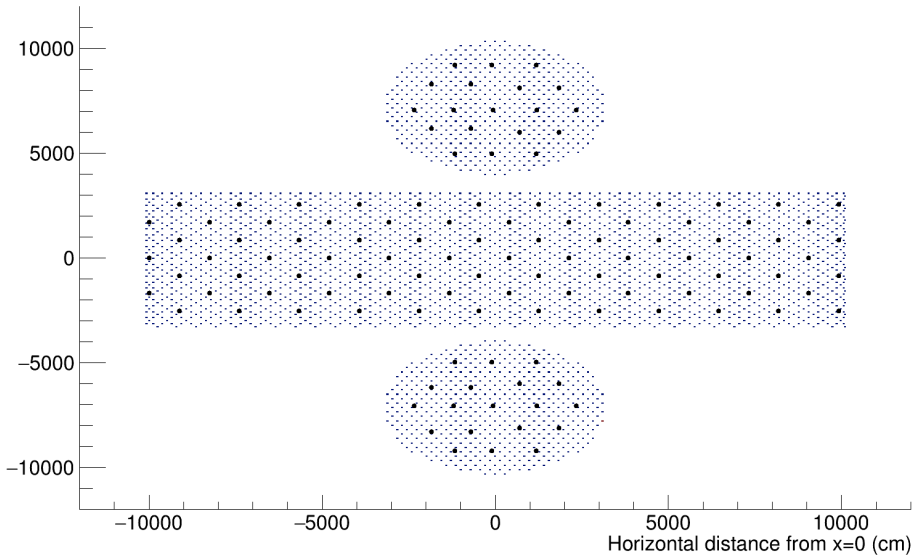
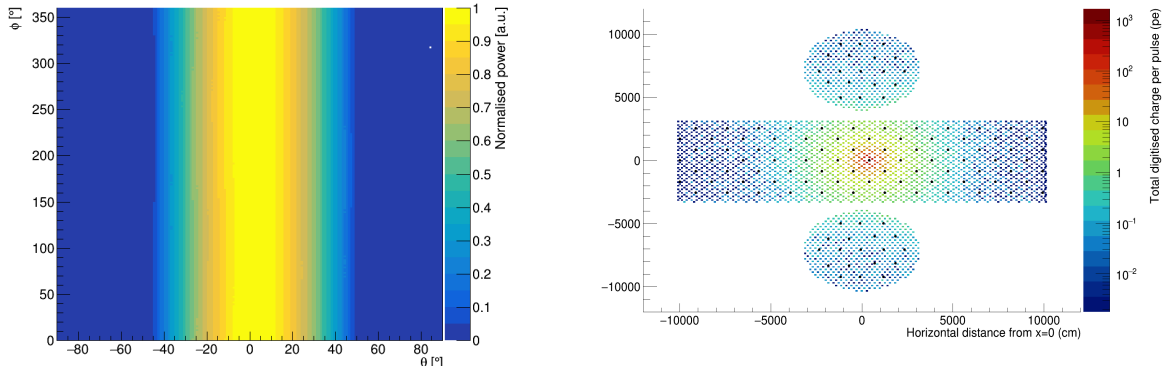


Figure 1: Positions of the OD PMTs and diffuser positions used in the calibration simulations. Note that the positions of PMTs in the top and bottom rows of the barrel have changed in the design, and as such the results presented in this tech note reflect these changes. This differs from the most recent version of WCSim (1.12.26) [4] that has been used as a basis for the simulation, and the changes are reflected in pull request #525.

- 143 • LI profile in the form of arrays of θ , ϕ and measured light intensity, where θ is the
144 angle made with the axis of the LI and ϕ is the rotation around the axis.

145 The LI profile opening angle and intensity can reflect either a flat angular distribution
146 of photons within the desired angular range of the light injector (-opening angle, +opening
147 angle), or can be drawn from the measured profile for that injector, in which case the LI
148 generator accurately models the variation across the profile, and in particular the drop-off
149 in the frequency of photons towards the edge of the LI profile. For each pulse, the generator
150 samples the specified number of photons per pulse, each with an energy calculated from the
151 wavelength set in a database currently stored within WCSim, and a time sampled from a
152 Gaussian distribution around the mean, with a variance equal to the pulse width specified
153 in the database. Each photon is also assigned a global direction, which is sampled with a
154 distribution corresponding to the LI profile.

155 The profile of each diffuser will be measured and stored in the database as a function
156 of the diffuser identifier number in the final simulation. For the purposes of the diffuser
157 simulations presented in this tech note, a single profile taken from the measurement of a
158 diffuser profile in water has been used. This diffuser profile corresponds to an opening angle
159 of around 40°. Since the OD diffuser profiles have not yet been measured in water, an ID
160 diffuser profile has been used to approximate a realistic OD diffuser profile. Although the
161 design of the OD diffusers has been modified from the ID diffuser design in order to increase
162 the diffuser efficiency, the design has been shown to maintain the desired profile and as such
163 the ID diffuser profile is expected to be a reasonable approximation. The diffuser profile
164 used, and the resulting charge map from a diffuser in the barrel is shown in Figure 2.



(a) ID diffuser profile measured in water, used for the diffuser simulations described in this technical report. A measured profile for each diffuser will be stored in the database for OD calibration.

(b) Charge in photoelectrons on each PMT produced when the profile in (a) is used to simulate optical photons from a diffuser pointing outwards in the barrel OD. The size of the PMT + WLS plates has been increased only in the plot for improved visualisation.

Figure 2: Diffuser profile measured in water, and the resulting charge map from this profile.

165 3.2 Diffuser and OD Parameters

166 The characteristics of diffusers simulated in the saturation study are summarised in Table I.
 167 The number of photons per pulse used in the simulation was based on measurements made
 168 from the LED pulser setup, using a chain of fibre optic cables equating to 181 m in length.
 169 The simulations described here use a maximum photon yield from the fibre optic chain of
 170 11 M photons per pulse. This was modified to account for an assumed diffuser efficiency of
 171 50%. As such, the simulated number of photons per pulse is 5.5 M.

Parameter	Assumed value
Photons per pulse	11 M
Wavelength	365 nm
Pulse width	10 ns
Diffuser efficiency	50%

Table I: The LI configuration used in the diffuser simulations for the saturation study presented in Section 3.3.

172 The OD geometry parameters that have been used in the simulations for the saturation
 173 study are shown in Table II.

174 3.3 Saturation Study

175 The limit of the PMT range is governed by the electronics response, which is expected to
 176 fully saturate at around 100 photoelectrons (pe) in a 16 ns time window. The simulation
 177 of the PMT charge response in WCSim does not currently handle the saturation, but it is
 178 expected that the linearity of the charge response will break down between 80 pe and 100 pe.
 179 Saturation measurements aim to measure the PMTs over the full range of this breakdown
 180 in linearity. The saturation level for the purposes of this study has been taken to be 100 pe
 181 in 16 ns, but the analysis has been designed to take into account the need to measure across
 182 the entirety of this range.

183 The saturation of OD PMTs has been evaluated in the top endcap, barrel and bottom

Parameter	Assumed value
PMT radius	8 cm
PMT dark rate	0.4 kHz
OD lateral water depth	1 m
OD height water depth	2 m
OD dead space	60 cm
Tyvek sheet thickness	1 mm
WLS plate thickness	6 mm
WLS plate length	30 cm

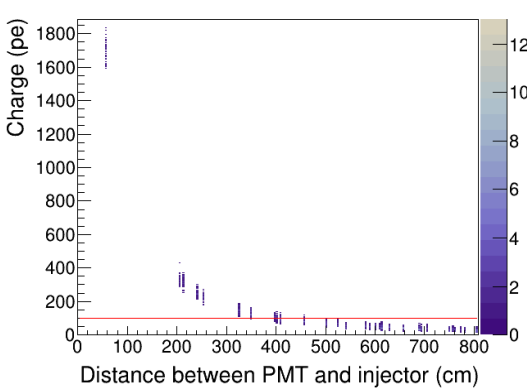
Table II: The OD configuration used for the saturation study presented in Section 3.3 using WCSim version 1.12.26.

endcap. The diffuser simulations are intensive, requiring millions of tracked photons to simulate a single flash. As such, only two diffusers in each of the top endcap, barrel and bottom endcap have been simulated for this current study.

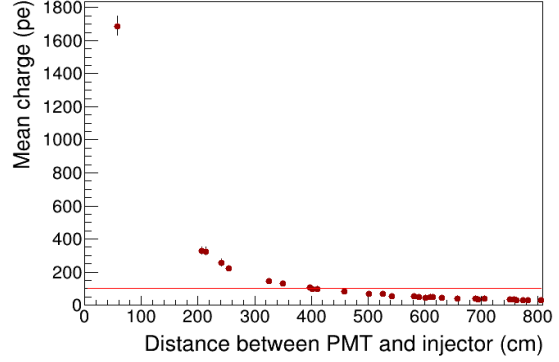
Two values have been used as figures of merit to determine the PMT saturation coverage:

- Mean saturation distance - the distance from the nearest diffuser at which the mean charge per PMT is greater than saturation level.
- Saturation limit - the greatest distance from the nearest diffuser at which the charge on any PMT reaches the saturation level.

For each configuration, the charge per PMT was plotted as a function of the distance from the nearest diffuser, to give the saturation limit (Figure 3a). The mean saturation distance was then found by taking the mean of the same plot (Figure 3b). The plot showing the saturation limit is particularly useful in understanding the range of distances over which it is possible to see the expected range of breakdown of linearity.



(a) Plot of the charge per PMT as a function of the distance from the nearest diffuser. The saturation limit is the greatest distance at which saturation is achieved i.e. 5.0 m in this case.



(b) Plot of the mean charge per PMT found by taking the mean of the left-hand plot. The mean saturation distance is the greatest distance at which the mean charge per PMT is greater than the saturation level i.e. 4.0 m.

Figure 3: Sample plots showing the mean saturation distance and saturation limit used as figures of merit for the saturation study. The red, horizontal lines mark the assumed saturation level of 100 pe.

Since only six diffuser locations have been simulated, the percentage of PMTs within the mean saturation distance and saturation limit is calculated assuming symmetry both of

199 the detector and of the diffuser positions with respect to the PMTs. However, for practical
 200 reasons, the diffusers have to be positioned off-centre in the empty cells between PMTs, next
 201 to the struts on the PMT support structure. As such, a full simulation of all diffusers should
 202 be performed in future, once the OD geometry and LI specifications have been finalised, for
 203 an accurate evaluation of the percentage saturation across the whole detector.

204 3.4 Results

205 The mean saturation distance and saturation limit were evaluated for two OD diffuser loca-
 206 tions in each of the top endcap, barrel and bottom endcap. These are shown in Table III,
 207 along with the percentage of PMTs within the mean saturation distance and saturation limit.
 208 Table IV shows the mean charge at the calculated saturation distance and the mean charge
 at the saturation limit at the six diffuser positions.

OD location	Mean saturation distance	% PMTs within saturation distance	Saturation limit	% PMTs within saturation limit
Barrel 1	4.0 m	31%	5.0 m	50%
Barrel 2	4.0 m	31%	5.0 m	50%
Top endcap 1	3.7 m	27%	3.9 m	30%
Top endcap 2	3.6 m	24%	4.3 m	37%
Bottom endcap 1	3.6 m	24%	4.3 m	37%
Bottom endcap 2	3.5 m	22%	6.1 m	66%

Table III: Results for PMT saturation using the diffuser configuration detailed in Table I.

OD location	Diffuser position	Mean charge (pe) at saturation distance	Mean charge (pe) at saturation limit $\pm 2\sigma$.
Barrel 1	(395.65,-3281.50,8.75 cm)	108	68 ± 12
Barrel 2	(3281.50,395.65,1705.55 cm)	105	67 ± 11
Top endcap 1	(-70.7,-97.3,3350.82 cm)	106	96 ± 14
Top endcap 2	(-707,-968.2,3350.82 cm)	108	77 ± 13
Bottom endcap 1	(-707,-968.2,-3350.82 cm)	108	77 ± 14
Bottom endcap 2	(707,-1157.8,-3350.82 cm)	114	42 ± 11

Table IV: Results for PMT saturation using the diffuser configuration detailed in Table I.

209
 210 Figure 4 shows the PMT charge map for the Barrel 1 diffuser, with the saturation distance
 211 and saturation limits marked around the barrel PMTs.

212 Due to the differing geometry the mean saturation distance in the barrel (4.0 m) is
 213 slightly higher than in the endcaps (e.g. 3.6 m), and the percentage of PMTs within the
 214 mean saturation distance in the barrel is higher at 31% than in the endcaps (22-27%).
 215 Similarly, the percentage of PMTs within the saturation limit in the barrel is higher than in
 216 the endcaps, with the exception of the bottom endcap 2 diffuser, with 66% of PMTs within
 217 the saturation limit of 6.1 m. It should be noted that changes to the OD geometry, including
 218 the addition of PMTs in the endcaps, are possible, and have not been taken into account in
 219 this simulation.

220 The diffuser position with respect to the surrounding PMTs has an observable effect
 221 on the saturation levels achieved. Where the diffuser positions with respect to surrounding
 222 PMTs are equivalent, as in the case of the two barrel diffusers, as well as the Bottom Endcap 1
 223 and Top Endcap 2 diffusers, saturation levels are largely the same. However, the positions of
 224 the Top Endcap 1 and Bottom Endcap 2 diffuser each differ from all other diffusers simulated,

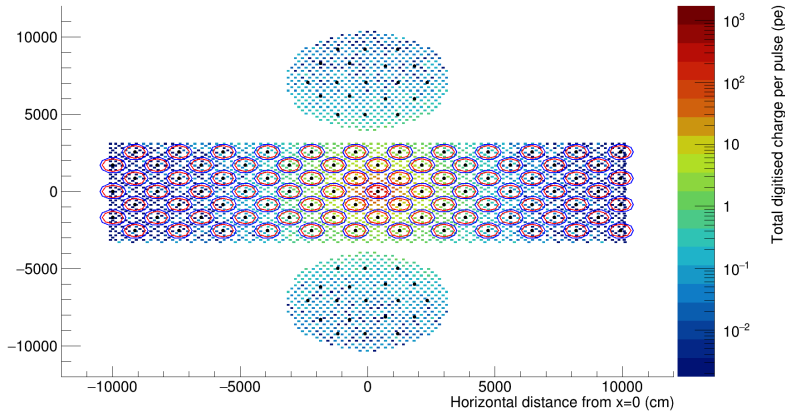


Figure 4: Charge in pe on each PMT as a result of illumination with the Barrel 1 diffuser. The mean saturation distance and saturation limit around each PMT in the barrel are marked in red (smaller circles) and blue (larger circles) respectively.

resulting in different saturation distances and saturation limits. Again, a full simulation of all diffuser positions should be carried out to fully evaluate achievable saturation across the whole detector, once all parameters and geometries have been finalised.

4 Diffuser Design

4.1 ID Diffuser Hemisphere Design

4.1.1 Inner Detector Diffuser Design

The diffusers used to scatter input laser light in the inner detector volume are 2.54 cm half-spheres fabricated from PTFE. This is used as it

- is unaffected by immersion in water
- acts as a excellent diffuser
- is a good transmitter of UV light
- is easy to machine and clean

A mechanical drawing of the inner detector diffuser hemispheres is shown in Figure 5

4.1.2 Diffuser Profile Measurement System

A scanning system was built to measure the output characteristics of diffuser hemispheres. Enclosed in a dark box, the diffuser is mounted onto two rotary stages which gives the freedom to rotate the diffuser around the nominal axis linking the diffuser with the photosensor. This scanner only takes scans in an air medium, and the setup is illustrated in Figure 6.

A laser powered from a wall plug is used to illuminate the diffuser with light at a wavelength of 450 nm. It is triggered by a function generator with 1000 triggers per burst at a frequency of 2 kHz. The open beam is directed via a mirror, a circulator, and a lens to the fibre launch stage, and then via an optical fibre towards the diffuser. The diffuser enclosure is fixed with three screws on the double-rotation stage. Measurements of bare diffuser profiles, i.e. without enclosure, are conducted with the bare fibre end positioned in the centre of the

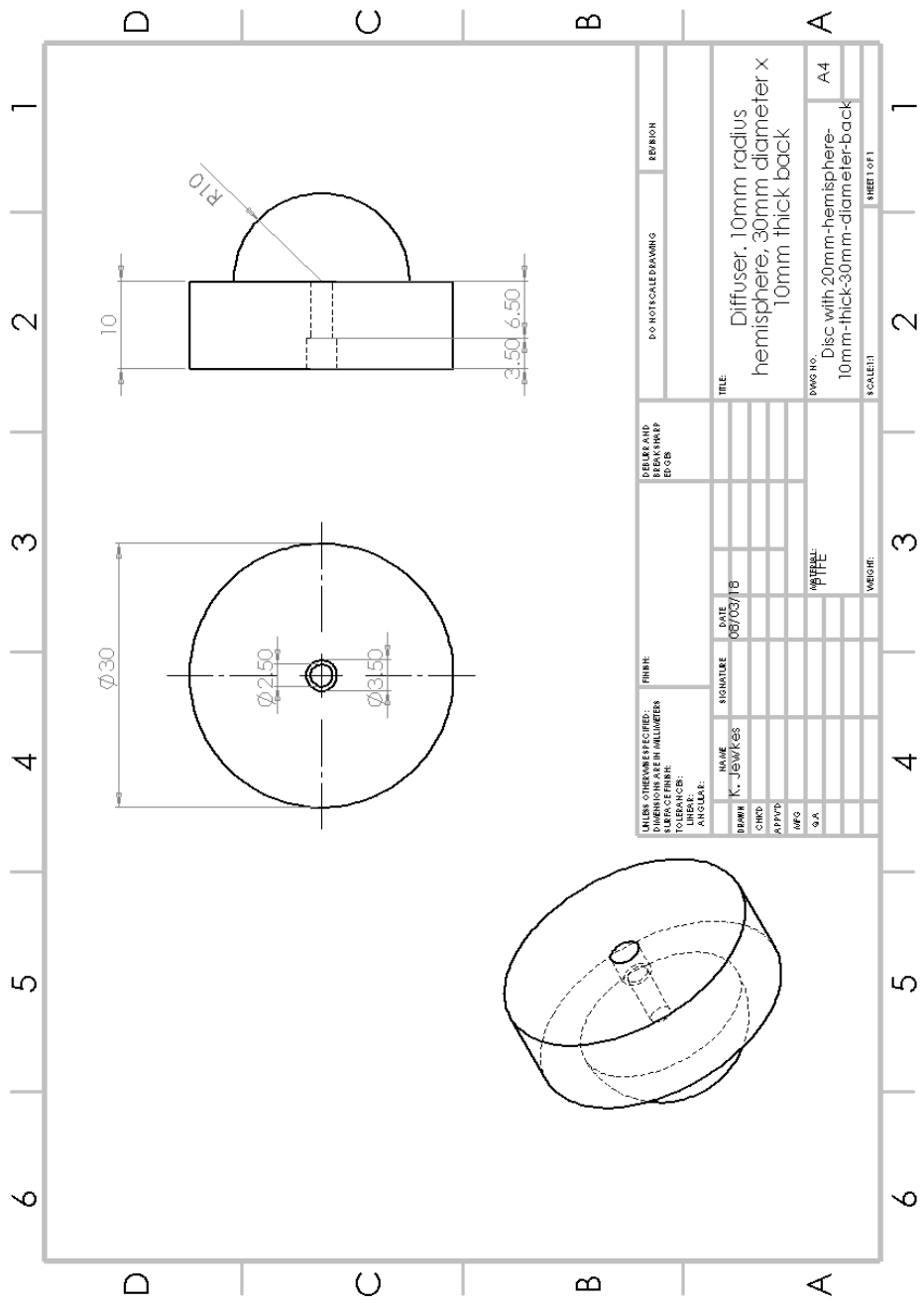


Figure 5: Bare Diffuser Mechanical Drawing

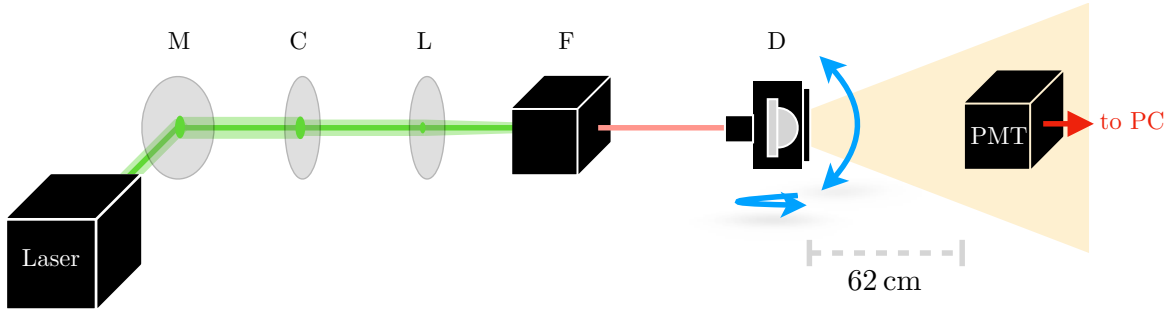


Figure 6: Setup for diffuser scans: light from the laser is directed via a mirror (M), a circulator (C), and a lens (L) to the fibre launch stage (F). From there, the light goes via an optical fibre to the diffuser (D) on the rotation stage.

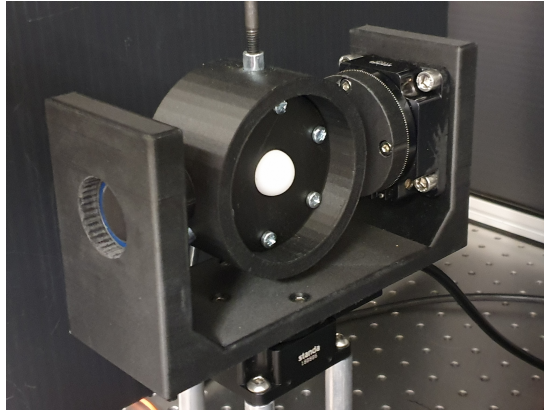


Figure 7: Rotation stage with bare diffuser hemisphere mounted using a 3D-printed frame.

rotation stage using a 3D printed frame. The bare fibre end is kept in place due to friction on the connection point with the diffuser hemisphere. A photograph of the rotation stage with a bare diffuser hemisphere is shown in Figure 7.

A PMT measures the diffuser spectrum at a fixed position, with 62 cm distance to the diffuser enclosure and a 3 mm pinhole aperture, restricting the solid angle viewed by the PMT to $2 \cdot 10^{-5}$ sr. For comparison, a single 50 cm PMT in the HK far detector receives light from a point source at the other side of the tank over a solid angle of approximately $2.2 \cdot 10^{-4}$ sr. The PMT signal is digitised at a sampling rate of 2500 MHz over 1000 cycles, allowing to resolve the shape of each single signal waveform. The light yield at each coordinate is then obtained as the average waveform area across all digitised signals.

The diffuser profile measurement system is discussed in detail in [5].

4.1.3 Diffuser Power Measurement System

In addition to the profile measurement functionality, the integrated power output from the diffuser was measured using an integrating sphere from Ophir. This sphere provides an unbiased measurement of the total light output power of any light source, regardless of the shape of the emission profile. A bespoke diffuser holder suitable for connection to one of the integrating sphere ports was 3D-printed, as was a holder for the optical fibre from the laser source.

A bare PTFE hemisphere was mounted into this holder and connected into the integrating sphere port. The bare end is inserted into the connection point in the same manner as for a bare profile scan. Tape was used to prevent light leaking out of the back

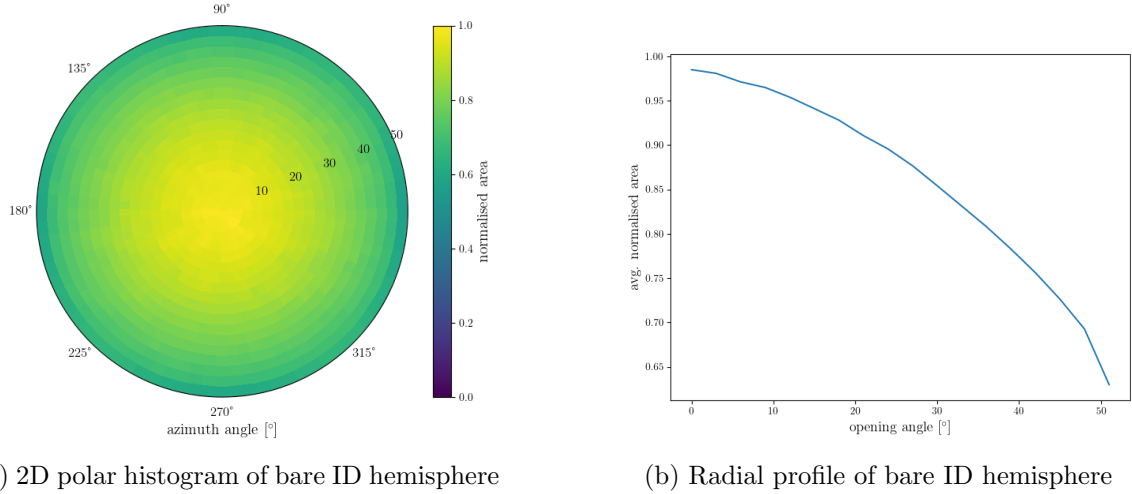


Figure 8: Profile scan of a standard bare ID diffuser hemisphere

of the hemisphere during the measurement, which also helped to keep the fibre in place. The hemisphere was then illuminated with light from the same laser, this time running on a continuous rather than burst setting. On the continuous setting light is supplied in a sinusoidal manner at a frequency of 1 kHz. Power measurements were taken once per second for a period of ten seconds to account for small fluctuations in laser intensity, the mean of which served as the final power measurement for that hemisphere.

In order to calculate a power ratio, a measurement of power for the bare fibre also needed to be obtained. This was done in a similar manner to a power measurement for a hemisphere, using the same laser and data acquisition settings. To make the comparison between fibre and hemisphere measurement as accurate as possible, a special hemisphere was created with the fibre connection point extended into a hole that runs through the length of the hemisphere. The bare fibre can then be inserted all the way through until it pokes out of the front, allowing a power measurement for the bare fibre to be taken with the conditions inside the integrating sphere as close as possible to hemisphere measurements. The ratio of hemisphere power to fibre power can then be taken to determine the amount of light lost.

A table of systematics for the power ratio measurement is shown in Table V. Rotation refers to changing the orientation at which the diffuser is placed into the holder, and diffuser re-insertion refers to removing the diffuser from the holder and replacing it. Fibre re-insertions refers to disconnecting and re-connecting the fibre into the diffuser, while bare fibre refers to dis- and re-connecting the fibre when taking bare fibre measurements. This results in a total systematic of 5.3% for a diffuser measurement and 1.8% for a fibre measurement, and therefore an uncertainty of 5.6% in a power ratio measurement.

Systematic	Std. dev. (%)
Rotation	1.4
Diffuser re-insertion	1.0
Fibre re-insertion	5.0
Bare fibre re-insertion	1.8

Table V: Integrating sphere systematics for the power ratio measurement.



Figure 9: A prototype of the OD diffuser with a 2 mm top hat.

292 4.2 OD Diffuser Design

293 The original intention was to use the same diffuser hemisphere design for the OD diffusers
 294 as will be used for the ID diffusers. However, the standard diffuser emits less than 20% of
 295 the power delivered by an optical fibre. As there are a number of interfaces in the optical
 296 pathway between the light source and the diffuser, and as the light source for the OD will be
 297 LEDs, this was considered too low to be able to effectively illuminate the OD space. Neither
 298 the number of interfaces in the optical chain, nor the light source can be changed easily, but
 299 it is possible that an alternate design of the diffuser hemisphere could yield more light.

300 Light is lost to two mechanisms in the standard diffuser; absorption by the PTFE and
 301 backscattering. Both loss mechanisms would be minimised if there were less PTFE in the
 302 light path. The design for the OD diffuser section was modified to be the shape of a top
 303 hat, as shown in Figure 9. The optimal depth was studied by taking profile and power
 304 ratio measurements using the same diffuser, but at smaller and smaller depths; after each
 305 measurement was completed, 2.0 mm was cut from the top-hat, and the measurements were
 306 re-taken. This procedure was repeated until the top-hat was 2.0 mm high.

Top-hat depth (mm)	Power ratio (%)
10.0	19.2
8.0	32.4
6.0	31.5
4.0	42.1
2.0	55.2

Table VI: Power ratio measurements for each depth of the top-hat

307 Results of the power ratio measurements are shown in Table VI. As expected, power ratio
 308 increases with decreasing top-hat depth, making the optimum depth 2.0 mm. The profile as
 309 shown in Figure 10 confirms that the shape of the profile is still suitable.

310 Based on these studies, we propose to change the OD diffuser design from a hemisphere
 311 to a top-hat with a 2.0 mm height above the base. The diffuser will still be fabricated from
 312 PTFE, but this new design (i) emits more light at higher emission angles (ii) doubles the
 313 amount of light that is emitted for a given LED power setting and (iii) is significantly easier
 314 to fabricate in bulk.

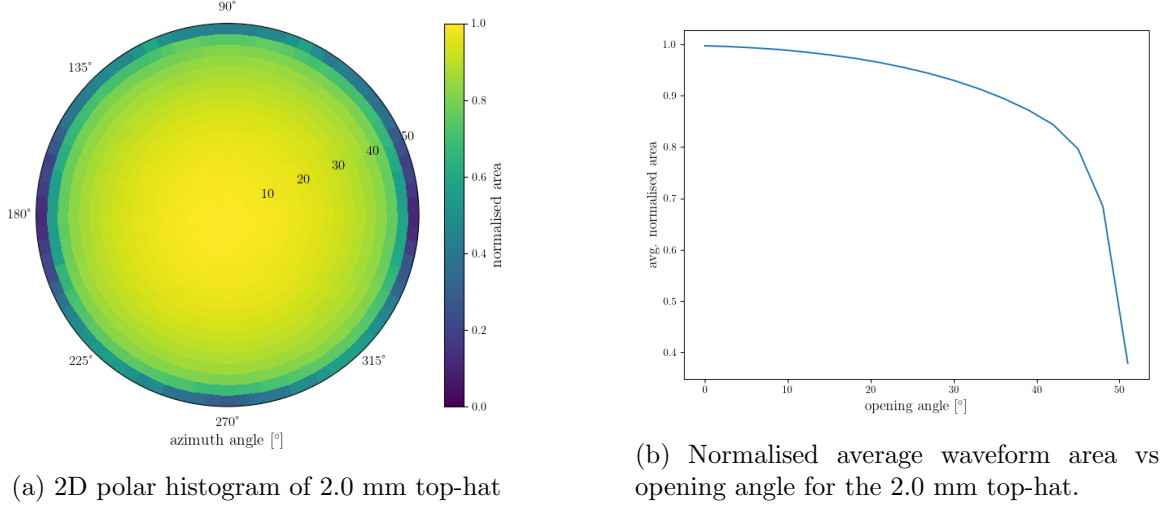


Figure 10: Profile scan of the 2.0 mm top-hat



Figure 11: (left) Front view of the prototype of the OD diffuser mount and (right) rear view of the prototype of the OD diffuser mount.

315 5 OD Diffuser Mounting System and Installation

316 The OD space will be illuminated by a total of 122 OD diffusers, 19 on each of the top and
 317 bottom caps, and 84 in the barrel. The barrel diffusers are distributed in 7 vertical layers
 318 each consisting of 12 OD diffusers. Due to the numbers and cost, the mounting system must
 319 be relatively small, easy to fabricate and easy to install. Installation will be carried out by
 320 workers on the gondola in the OD space after the Tyvek has been installed and as the fibres
 321 are being installed. The gondola worker will install the fibre in the OD diffuser, and fix the
 322 mount to the HK frame, oriented into the OD space. Since this is being done on the gondola,
 323 the mount needs to be small, easy to store, and straightforward to install.

324 Drawings for the OD diffuser prototype mount can be seen in Figure 11 and pictures
 325 of the prototype can be seen in Figure 12. The mount is made from stainless steel and is
 326 designed to hook over a horizontal frame bar, and screw in from the bottom. The PTFE
 327 mount is approximately 5 cm on a side. The fibre will be installed from the back and is held
 328 in place by a T-shaped component that is screwed down by the gondola worker.

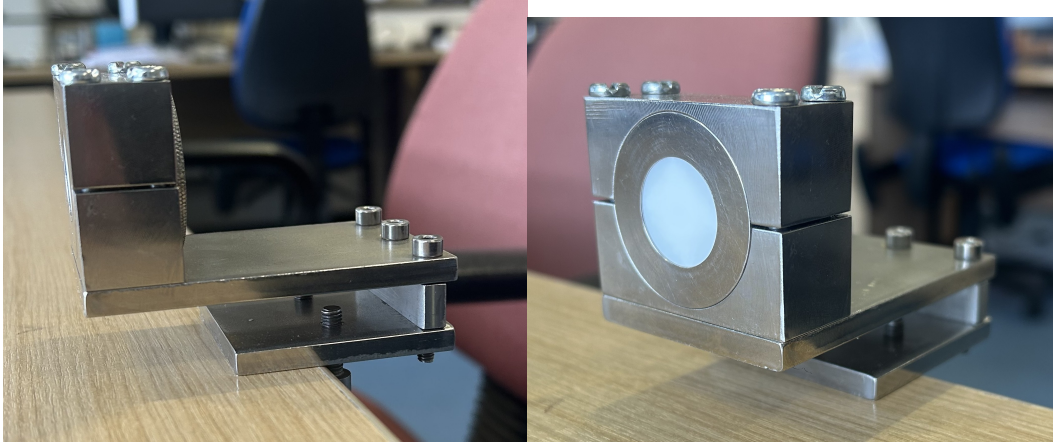


Figure 12: (left) Side view of the prototype holder and (right) front view of the prototype holder.

329 **6 Pulser Board**

330 **6.1 Pulser Board Overview**

331 The pulser board was designed to be a more efficient and compact version compared to
 332 Super-Kamiokande UK Light Injection system, improving on efficiency, functionality, and
 333 light output. The pulser board is a rather simple board designed for low cost production.
 334 This section explains each circuit, component selection and design decision. As of writing,
 335 the board development is v0.9. v1.0 will be ready by September and will have only minor
 336 changes and adjustments compared to v0.9, mostly centered on refinement and removing the
 337 prototyping circuit.

338 **6.2 Physical dimensions and construction**

339 The dimensions of the Printed Circuit Board (PCB) were selected to be as compact as practicable, while still providing sufficient area for the secure mounting of a fibre coupler and for
 340 the components. The final board size is 50 mm × 30 mm. This configuration permits electrically noisy components, such as switching power supplies and the Low Voltage Differential
 341 Signal to Transistor Transistor Logic (LVDS-to-TTL) converter to be positioned at a maximum
 342 distance from the switching circuitry, thereby minimising potential electromagnetic
 343 interference.

344 Although it is technically feasible to further reduce the board size, preliminary design
 345 studies and practical build indicated no substantial benefit in doing so. The board density
 346 cannot be significantly increased inside the crate due to FPGA LVDS count and Eurocard
 347 dimension, and cost analyses revealed negligible differences associated with a smaller PCB
 348 footprint. Furthermore, the chosen dimensions provide an adequate area for the fibre coupler
 349 and the necessary mounting holes to affix the pulser board onto the Eurocard, thereby
 350 ensuring reliable optical alignment and mechanical stability. The PCB is fabricated as a four-
 351 layer FR4 [6] board with a thickness of 0.8 mm, in accordance with the standard construction
 352 offered by PCB Train/Newbury Electronics¹, see Figure 13. Refer to Figure 14 for the 3D
 353 model of the pulser board. The Top Layer and Inner Top Layer are shown in Figure 15, and
 354 the Inner Bottom Layer and Bottom Layer are likewise illustrated in Figure 16. A combined
 355 view of all PCB layers is provided in Figure 17.

¹These are trading names of the same manufacturer.

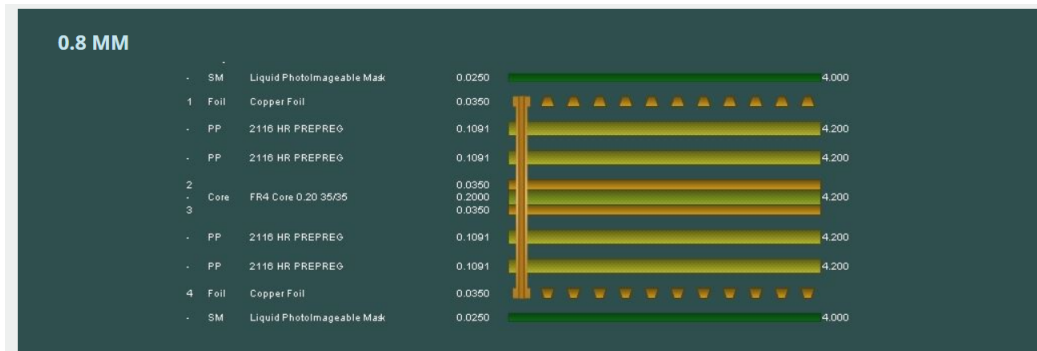


Figure 13: PCB Train's 4 Layer 0.8mm Layer Stack

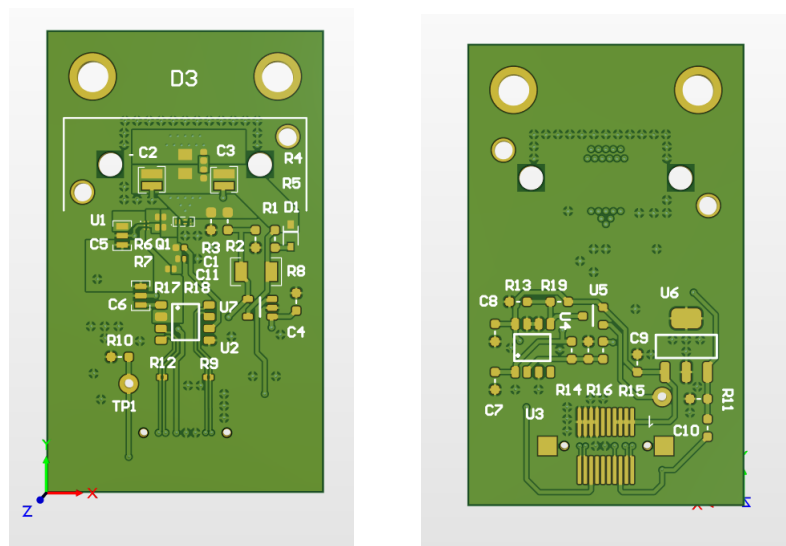


Figure 14: Pulser Board's 3D view Top and Bottom

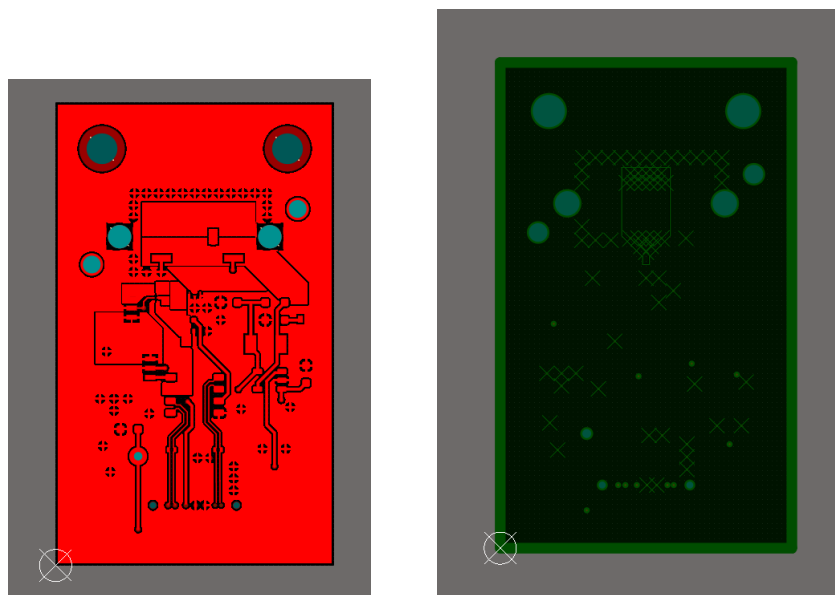


Figure 15: Pulser Board Top and Inner Top Layer

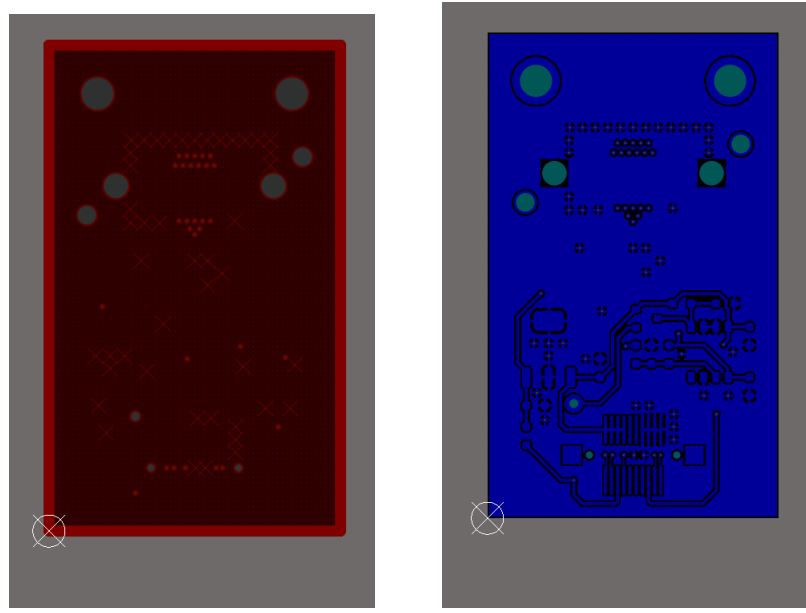


Figure 16: Pulser Board Inner Bottom and Bottom Layer

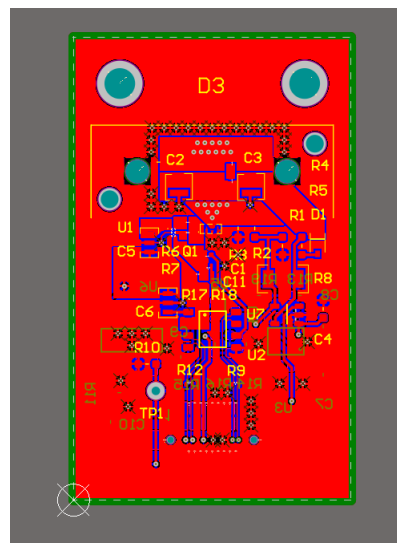


Figure 17: Pulser Board Layer Overview

358 **6.3 LED**

359 **6.3.1 Overview**

360 The LEDs are the most crucial component in the system as the characteristics of these
 361 primarily determine the light output, regardless of electronics. LEDs are usually not rated
 362 for such high-speed applications, which meant LEDs had to be tested and validated in-house,
 363 as datasheets do not provide the required information. The specification required was a 1–
 364 10 ns clean single pulse, sub-400 nm wavelength, small surface mount package, narrow output
 365 beam so it can be coupled to a fibre with reduced losses and a good range of photon output.
 366 Several LED packages were purchased from Kingbright and LC-LED, and their performance
 367 tested. The results of these tests are given in Section 6.3.4.

368 **6.3.2 Switching Circuit**

369 The redesign process provided a valuable opportunity to evaluate a revised layout and new
 370 components for the switching circuit. Several enhancements have since been implemented
 371 in the revised switching circuit. Most importantly, the switching side of the layout has
 372 been rerouted. In contrast to the previous configuration, where current would flow through
 373 the limiting resistor regardless of the LED state, the updated design only allows current
 374 flow when the LED is active (refer to Figure 18). This modification reduces both thermal
 375 dissipation and the overall power consumption of the system. To modulate light intensity,
 376 a variable power supply is now employed to adjust the voltage supplied to the LED. This
 377 method has proven highly effective. Tests were conducted at various voltage levels using
 378 the full 181 m length of optical fibre—the maximum expected in Hyper-K at the time of
 379 testing—and the resulting photon output ranged from approximately 1×10^5 to 2×10^7
 380 photons per pulse. Refined testing results are shown in Section 6.3.4. Further discussion
 381 regarding the implementation and performance of the variable voltage supply is provided in
 382 Section 6.5.

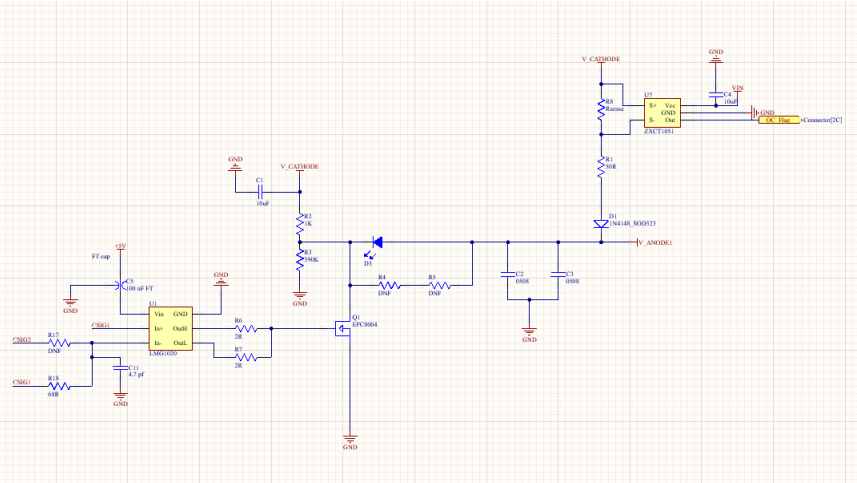


Figure 18: Switching Circuit Layout with LMG1020 and over current IC, R4 is 6.8 nH inductor and R5 is 3R3 resistor

383 **6.3.3 Switch Selection**

384 The previous iteration of the pulser board utilised a BFR92 [7] high-speed RF NPN switching
 385 transistor which was directly driven by a LVDS-to-TTL converter. In the redesign phase,

386 alternative circuit topologies were explored—particularly those suitable for generating (sub-
387)nanosecond pulses. This investigation led to the adoption of gate driver circuits. Gate
388 drivers are advantageous not only because they can power switches with challenging drive
389 requirements, but also because sub-nanosecond electrical pulses can be achieved by modu-
390 lating the enable pin with slight timing offsets.

391 The fastest commercially available gate driver identified was the Texas Instruments
392 LMG1020 [8]. This device supports pulse widths down to 1 ns, with typical rise and fall
393 times of 400 ps. Additionally, it features an enable pin that allows for precise nanosecond
394 pulse shaping ². The LMG1020 is compatible with both Gallium Nitride Field Effect Tran-
395 sistor (GaN) and Metal Oxide Semiconductor Field Effect Transistor (MOSFET) switches,
396 broadening the scope for future component integration and experimentation. It is widely
397 available and priced at £1.97 per unit in the quantities we will require for full production.

398 For the switching element, enhancement-mode GaN transistors manufactured by EPC
399 were selected due to their superior switching characteristics. This recommendation originated
400 from Nick Braam, an engineer at the University of Victoria, who contributed to the pulser
401 board design for the mPMT system. Two EPC devices were shortlisted: the EPC2012 [9] and
402 EPC8004 [10]. The EPC2012 offers a simpler footprint, which could reduce manufacturing
403 defects. However, the EPC8004 features lower parasitic capacitance, see Figure 19 for the
404 EPC2012 values and Figure 20 for EPC8004 values, leading to better high-speed performance.

405 To evaluate optical output performance, a 40 m length of FP400URT [2] optical fibre,
406 a Mouser-sourced 385 nm LED (ATS2012UV385 [11]), and a Hamamatsu H10721-210 [12]
407 PMT were used. The EPC-based configurations exhibited nearly identical pulse shapes,
408 whereas the BFR92-based circuit’s pulse shape was less sharp at identical pulse widths, as
409 shown in Figure 21. Consequently, the EPC8004 (Figure 22) was chosen for implementation.
410 Optimal performance of the EPC GaN switches required careful layout considerations. A
411 layout was developed in accordance with EPC’s design guidelines [13], targeting minimal
412 parasitic inductance and capacitance. The design employs two layers placed directly above
413 one another, utilising large copper planes and multiple vias to ensure uniform current dis-
414 tribution. The PCB will be fabricated and assembled by PCB Train, using their 0.8 mm
415 thick, four-layer stack-up, which offers minimal inter-layer separation for optimal electrical
416 performance (Figure 13). This same layout strategy was applied to the BFR92 circuit to
417 provide a fair performance comparison.

418 A significant challenge at low pulse widths is the presence of a trailing edge or “tail” in
419 the LED output. This effect arises due to charge accumulation and the intrinsic capacitance
420 of the LED, resulting in extended decay times and pulse broadening (see Figure 23). To
421 mitigate this, a parallel modified snubber circuit was implemented, consisting of a 6.8 nH
422 inductor and a 3.3 Ω current-limiting resistor. Upon LED turn-off, the inductor generates an
423 electromotive force (EMF) that actively extracts residual charge from the LED, accelerating
424 its shutdown. The effectiveness of this approach is illustrated in Figure 24. Additionally,
425 two 0508 reverse-topology 100 nF capacitors have been incorporated. Their role is to act as
426 local energy reservoirs, providing rapid current delivery to the LED during pulse operation,
427 surpassing the response time of the main power supply.

428 6.3.4 Testing

429 For testing purposes, the previous-generation United Kingdom Light Injection (UKLI) moth-
430 erboard and associated software were utilised in conjunction with a prototype of the next-
431 generation pulser board. This prototype consisted of four distinct circuit variants: one
432 employing the EPC8004 switch, another utilising the EPC2012 switch, a third using the

²See page 12 and 13 in [8].

PARAMETER	TEST CONDITIONS	MIN	TYP	MAX	UNIT
Dynamic Characteristics ($T_j = 25^\circ\text{C}$ unless otherwise stated)					
C_{ISS}	$V_{\text{DS}} = 100\text{ V}, V_{\text{GS}} = 0\text{ V}$		128	145	pF
C_{OSS}			73	95	
C_{RSS}			3.3	4.4	

Figure 19: EPC2012 Capacitance Values IC

PARAMETER	TEST CONDITIONS	MIN	TYP	MAX	UNIT
Dynamic Characteristics[#] ($T_j = 25^\circ\text{C}$ unless otherwise stated)					
C_{ISS}	$V_{\text{GS}} = 0\text{ V}, V_{\text{DS}} = 20\text{ V}$		45	52	pF
C_{OSS}			23	34	
C_{RSS}			0.8	1.3	

Figure 20: EPC8004 Capacitance Values IC

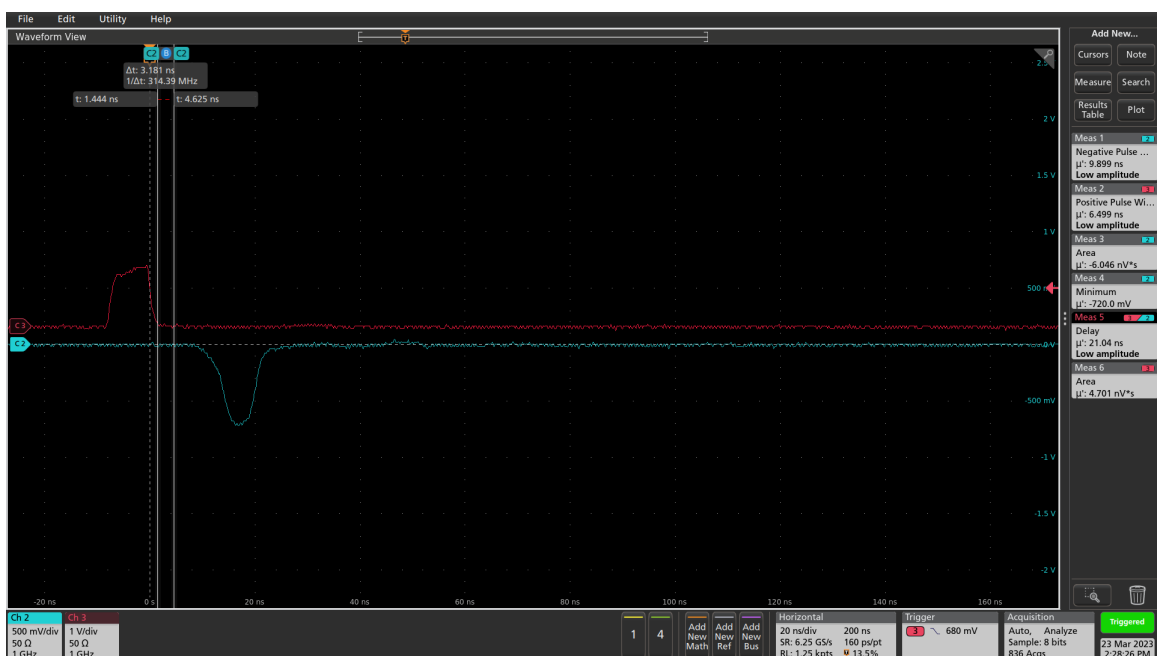


Figure 21: BFR92 Pulse Shape

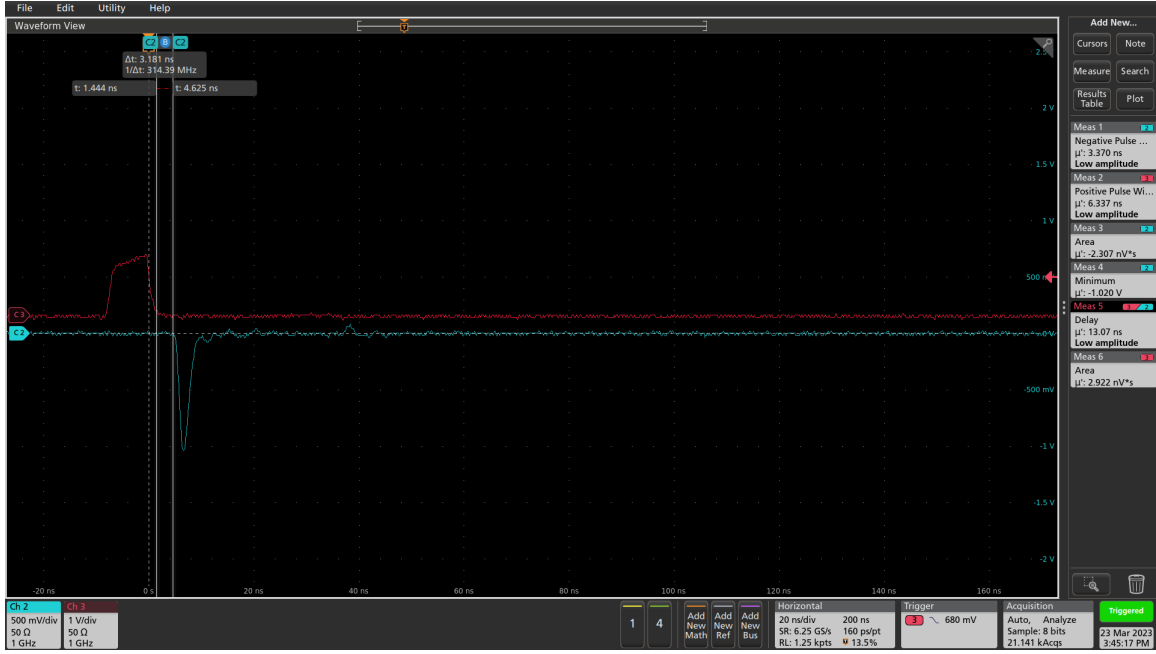


Figure 22: EPC8004 Pulse Shape

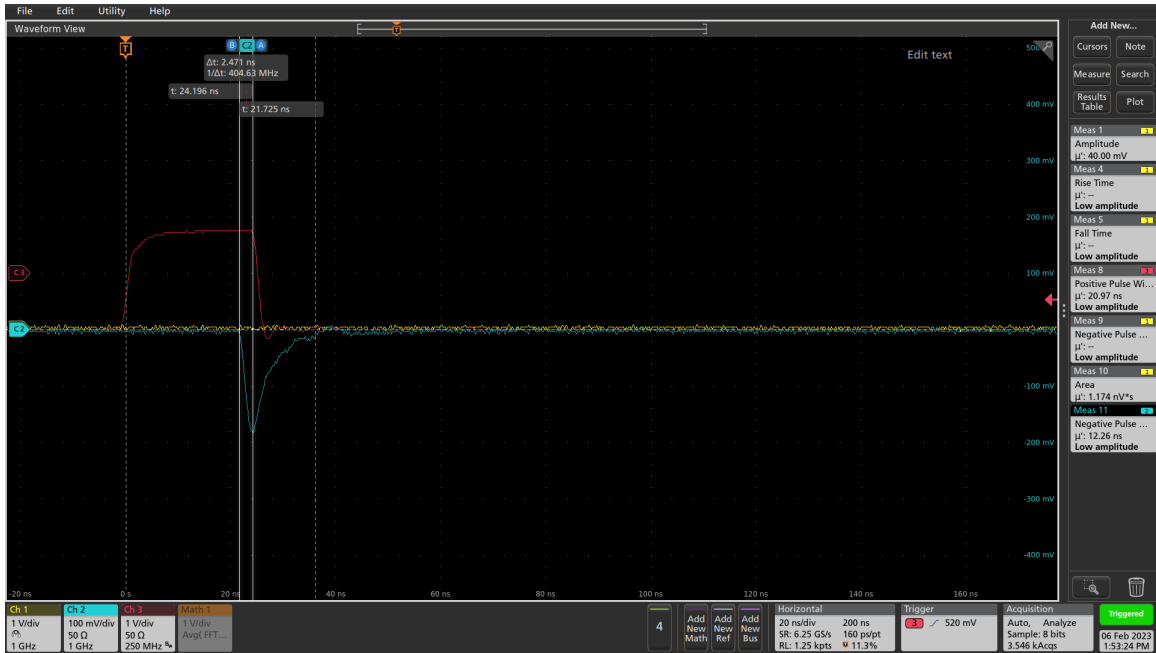


Figure 23: Pulsing Circuit With No Inductor and Resistor

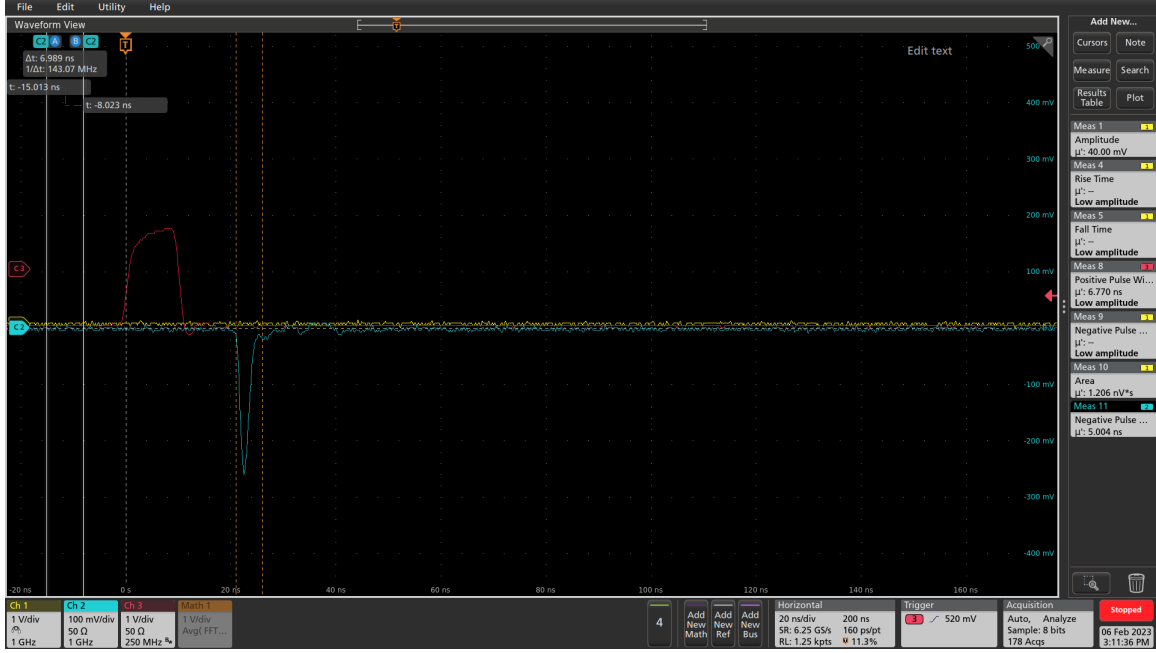


Figure 24: Pulsing Circuit With Inductor and Resistor

433 same high-speed transistor (BFR92) as implemented in the legacy system, and a fourth variant
 434 incorporating an EPC2012 gate in a through-hole package instead of the standard 0805
 435 surface-mount footprint. Further evaluation was also performed using the latest pulser board
 436 prototype once they had arrived.

437 Following comparative performance evaluations, the configuration using the EPC8004
 438 switch was selected for continued use. While both the EPC8004 and EPC2012 switches ex-
 439 hibited similar electrical characteristics, the EPC8004 offered superior performance due to
 440 its lower parasitic capacitance, without any additional cost. The pulser board assembly was
 441 housed within a dark box during testing, and a 3D-printed fibre coupler was employed to
 442 facilitate light delivery. The initial focus of the evaluation was on the shape of the gener-
 443 ated optical pulse. During component selection, it was observed that the LED previously
 444 sourced from Mouser (ATS2012UV385 by Kingbright) provided acceptable performance in
 445 terms of electrical characteristics, but the optical output was suboptimal. Additionally, this
 446 LED was found to be out of stock and obsolete at the time after testing, precluding further
 447 procurement. Subsequently, four ultraviolet LEDs from LC LED were assessed—two emit-
 448 ting at 365 nm and two at 395 nm—each in both 0805 and 0603 surface-mount packages.
 449 Results demonstrated that the 0805 package LEDs provided significantly better optical cou-
 450 pling efficiency with the FP400URT optical fibre. Furthermore, the 365 nm variant exhibited
 451 superior optical power output relative to the 395 nm counterparts. Based on these findings,
 452 the LC LED UT-67UV365P [14] 365 nm LED was selected as the most suitable LED for this
 453 application.

454 6.4 LVDS to TTL Converter

455 The DS90C402 [15] from Texas Instruments was selected as the LVDS-to-TTL conversion
 456 solution. This device is a dual-channel converter, chosen primarily for its fast switching
 457 characteristics—offering both rise and fall times of approximately 500 ps. It operates at
 458 5 V and provides 5 V TTL output levels, which aligns well with the requirements of the
 459 downstream switching circuitry. The inclusion of two channels is particularly advantageous,

as it enables the generation of sub-nanosecond differential pulses by precisely offsetting the channels, as described in Switch Selection. Among commercially available devices with these specifications, the DS90C402 is the fastest and is readily available through multiple distributors.

The associated circuit was implemented in accordance with the manufacturer's recommendations provided in the datasheet. A decoupling capacitor was placed in close proximity to the power supply pin to minimise voltage ripple. Output traces were routed using polygon fills to reduce impedance and enhance signal integrity, and a continuous ground plane was placed beneath the signal layers to improve shielding and minimise electromagnetic interference. The schematic for this is given in Figure 25.

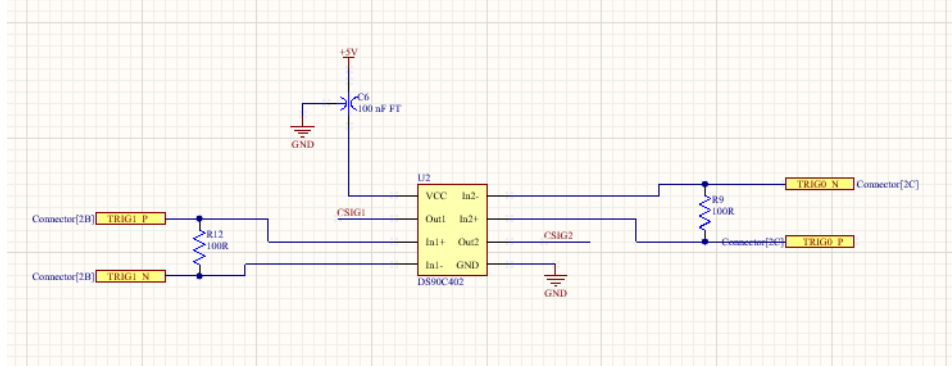


Figure 25: LVDS-TTL Converter Schematic

6.5 Power Supplies

Each pulser board is required to incorporate a variable voltage power supply dedicated to driving the LED, with an adjustable output range from 3 V to 12 V. This supply is used exclusively to modulate the LED's light output by varying the forward voltage, and consequently the current. The design specification also necessitates that the power supply be remotely controllable—i.e., capable of being switched on or off via a simple logic-level signal.

For this purpose, the LT1963A [16] adjustable low-dropout linear regulator was selected. This regulator has demonstrated reliable performance in previous pulser board iterations and offers a favourable balance of cost-effectiveness and controllability. The implementation includes standard filtering and decoupling, with layout details provided in Figure 26. The schematic provided in Figure 27 is an early version used for prototyping; the adjustable circuit has been simulated and will be tested shortly, and the enable circuit has been tested, modified and simplified. Updated schematics will be provided with v1.0 circuit.

In addition to the variable LED supply, each board requires a stable 5 V supply to power both the DS90C402 LVDS-to-TTL converter and the LMG1020 gate driver. Unlike the LED supply, this rail remains continuously powered. The 5 V supply is provided by an LM2937-5 [17], a fixed-output linear voltage regulator, which has been successfully employed in various high-speed and low-noise applications within the laboratory. The associated circuit schematic and layout and schematic are shown in Figures 28 and 29 respectively.

To meet system-level design constraints, each pulser board is equipped with its own independent 12 V input supply, ensuring that LED output intensity can be individually controlled on a per-board basis. However, the 5 V supply is common across all boards and derived locally on each pulser module. This approach allows for localised filtering and minimal power distribution path lengths, reducing the risk of noise coupling and voltage

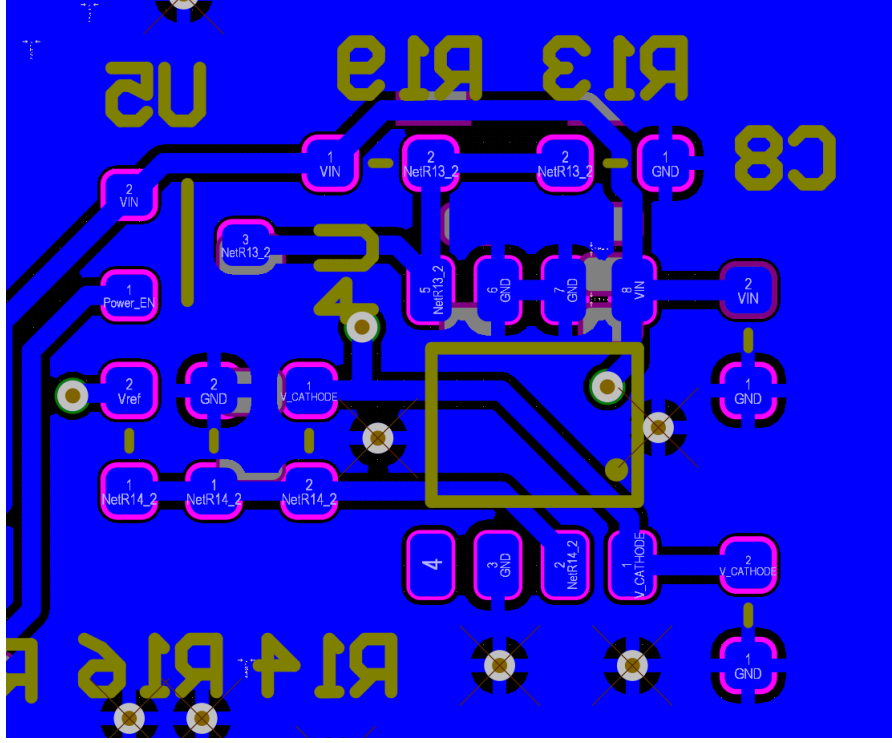


Figure 26: LT1963 Layout

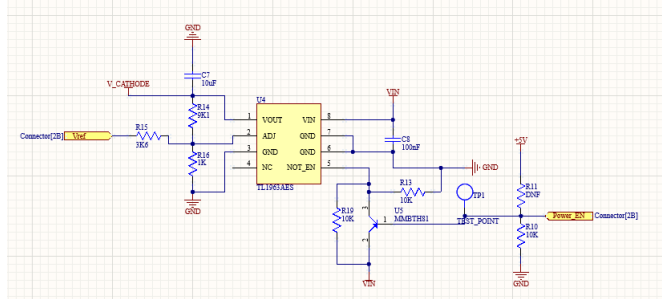


Figure 27: 12V Circuit Schematics

drop considerations that are particularly critical in high-speed circuit applications.

Power is supplied to each board via the Eurocard backplane. The 12 V input from the Eurocard simultaneously feeds both the variable (LED) and fixed (logic) power regulators on the pulser board. The LED enable function is controlled via a 5 V logic signal originating from the Eurocard's GPIO interface. Additionally, a DAC output from the Eurocard provides a voltage control signal to the adjustment pin of the LT1963A regulator on each pulser board, thereby allowing precise, programmable control of light intensity.

6.6 Connector

The previous board connector was deemed too bulky and expensive for the larger number of channels needed in this system, leading to the process of finding a more suitable alternative. Following an evaluation of commercially available options, the Phoenix Contact female connector 1331962 [18] was selected. This connector offers several advantageous specifications: it is rated for 500 V, features a low contact resistance of $40\text{ m}\Omega$, supports a maximum current of 0.5 A, and is capable of signal transmission up to 20 Gbit s^{-1} . In addition, it is

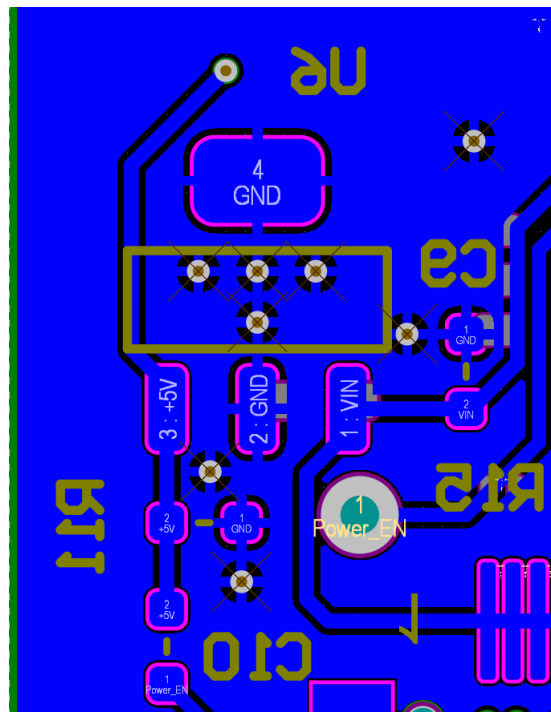


Figure 28: LM2937-5 Layout

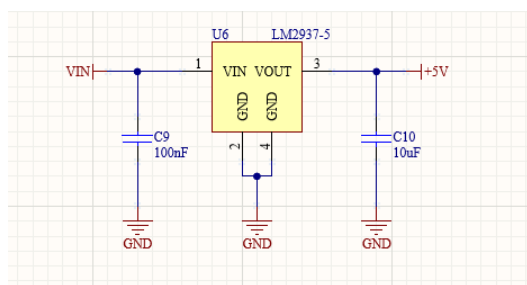


Figure 29: 5V circuit schematics

509 cost-effective, priced at approximately £0.50 per unit, with wide availability ensuring ease
 510 of procurement. Multiple height variants are available within the same series, facilitating
 511 flexible mechanical integration within the Eurocard crate system. The compact footprint of
 512 the connector allows for a reduced PCB form factor. Electrically, the high-frequency perfor-
 513 mance supports reliable LVDS signal transmission. Additionally, the compact footprint of
 514 the connector is well-suited to space-constrained PCB layouts.

515 An illustration showing the connector and corresponding circuit layout is provided in
 516 Figure 30.

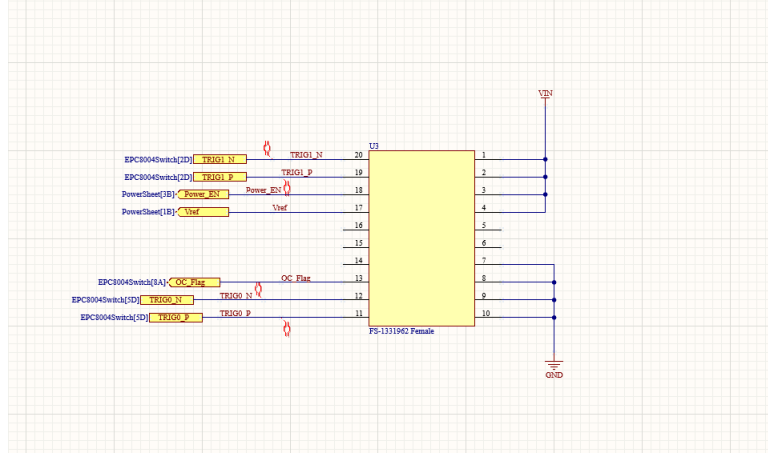


Figure 30: Connector Schematics

517 6.7 Fibre Coupler

518 During the prototyping phase, improvements were made to the PCB layout to better ac-
 519 commodate a fibre coupler. As a result, the current design includes provisions for precise
 520 mechanical mounting and alignment. Specifically, two mounting holes for M2 screws have
 521 been incorporated, enabling the 3D-printed coupler to be firmly secured to the board (see
 522 Figure 31). In addition, two dowel holes have been added to guide the coupler into posi-
 523 tion, ensuring accurate alignment over the LED. Given the tolerances associated with PCB
 524 fabrication and 3D printing, an alignment accuracy of approximately 100 µm is expected.



Figure 31: Old Fibre Coupler Design

525 To optimise the electrical path, capacitors have been repositioned as close as possible to

526 the LEDs. This minimises parasitic inductance and resistance, while enabling a centralised
527 layout of larger components. The resulting configuration creates a compact chamber housing
528 both the LEDs and associated capacitors.

529 An earlier design for the fibre coupler, which assumed uniform fibre lengths for all channels,
530 has since been abandoned. The current approach for the LED light injection system
531 adopts five different fibre lengths, necessitating individual light attenuation for each channel.
532 This attenuation will be implemented within the coupler itself, allowing the LED output to
533 remain within the electronically controlled dynamic range.

534 The proposed design is modular, consisting of three components: a base section mounted
535 to the pulser PCB, a top section into which the fibres will be epoxied, and an intermediate
536 attenuator element. The latter will serve to space the fibre from the LED and thereby adjust
537 the optical coupling efficiency to achieve the required attenuation. While an initial prototype
538 will be developed in the near term for functional testing, the full design and validation of the
539 fibre coupler will be undertaken later, once the required fibre lengths are fixed and unlikely
540 to change. Should the project timeline require faster iteration, this can be pursued.

541 The fibre coupler will be fabricated via stereolithography (SLA) using a black resin to
542 minimise light transmission through the material. Additional light-tight testing will be
543 conducted, and black paint may be applied if further sealing is required. Furthermore, laser-
544 cut rubber gaskets will be introduced at interface points to ensure optimal optical isolation
545 and mechanical sealing.

546 **6.8 Photon Yield Tests**

547 tests on maximising photon yield and available dynamic range should be fully described here

548 **6.9 Production**

549 Production will be carried out using PCB Train as they are local and competitively priced,
550 and known to produce boards of good quality. Estimated cost is £12.27 per board, which
551 equates to £1,496.94 for 122 units or £1,840.5 for 150 units, and production is £4073.48 for
552 122 units for 15 days lead time, or £3985 for 150 units at 25 days lead time. The full cost
553 breakdown is shown in Figure 32

554 **6.10 Changes Expected from v0.9 to v1.0**

555 **6.10.1 LED and Switching Circuit**

556 There will be minimal changes to the LED and switching circuit. Changes will be made to
557 the position of the switching devices, placing them slightly closer to each other to reduce
558 transmission line length. The LED will likely remain as the LC LED UT-67UV365P 365nm
559 0805 LED, but further LED tests will be performed. This takes a short amount of time, and
560 may lead to discovering better LEDs in the future which would be easy to swap in due to
561 standardised footprints.

562 **6.10.2 LVDS-to-TTL converter**

563 No changes are expected to this circuit.

564 **6.10.3 Power supplies**

565 Reverse voltage bias will be removed as no difference between normal and reverse bias was
566 observed photon output. The overcurrent protection and power enable circuit will be re-
567 worked.

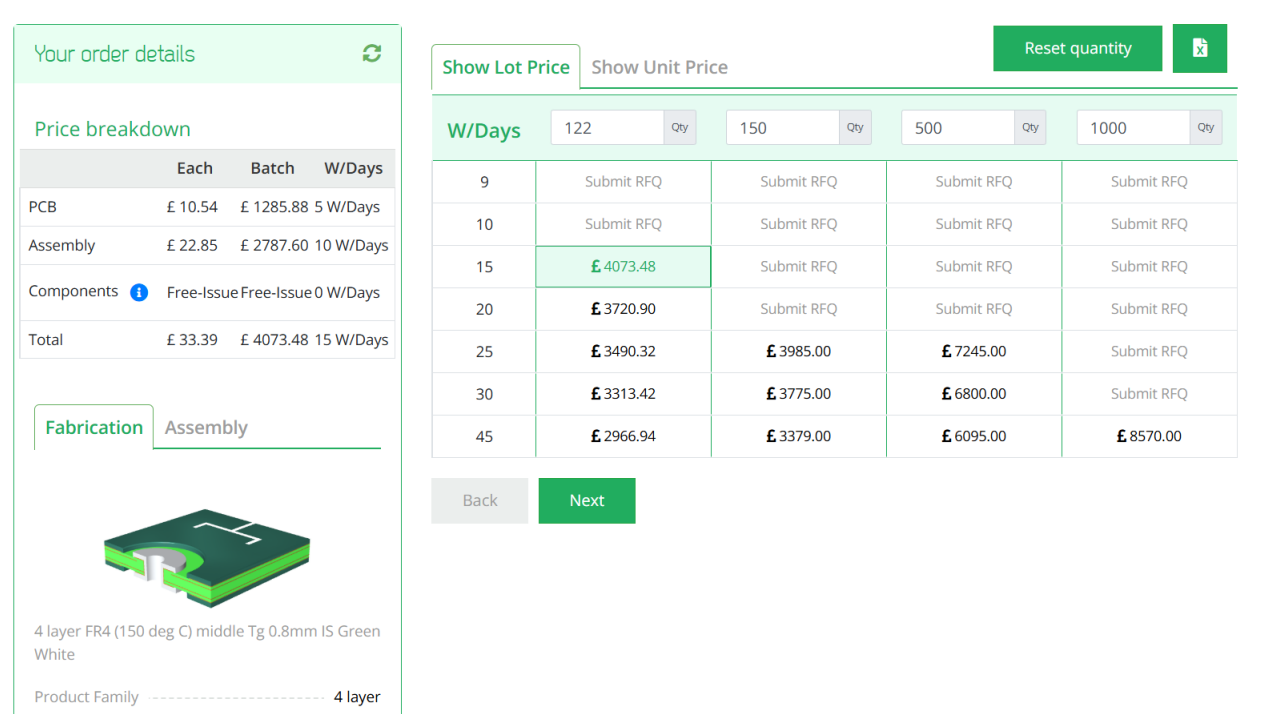


Figure 32: PCBTrain PCB production and assembly costs

568 6.10.4 Connector

569 No changes are expected to this.

570 6.10.5 Fibre coupler

571 A brand new fibre coupler will be designed due to the recent requirement changes regarding
572 the different fibre lengths.

573 7 Server Rack and Cooling

574 To house the electronics for the LI systems, two 42U server racks with 800 mm depth will
575 be used. The front of the server rack will be used for electrical connections and displays,
576 and the reverse/internal will be used only for fibre routing. The server racks will include
577 Uninterruptible Power Supplies (UPS) for safe power delivery and for power processing, to
578 avoid issues with potential instabilities in the main power supply. Each rack will include an
579 air conditioning unit to have a controlled temperature and remove humidity from the air,
580 as the relative humidity in the air is expected to be above 70%. Although specific tests on
581 running the LED electronics in humid conditions have not been carried out, it is known that
582 the optical switches for the laser calibration system requires lower humidity levels. In order
583 to simplify things and remove the potential of humidity issues with the LED electronics,
584 both server racks will be air conditioned. These systems are widely available and will be
585 chosen closer to installation.

586 **8 LED Monitoring**

587 To monitor the light output from the LEDs before attenuation by fibres and convolution
588 with water parameters, PMTs will be placed near to the LED sources. This is a similar
589 design to what is currently used in the Super-K UKLI system. Each LED connector will
590 feature a second fibre to take light to a series of PMTs, which are expected to be Hamamatsu
591 H10721-210. Due to the 8 mm diameter of the PMT window, up to 16 fibres can be attached,
592 meaning one PMT can monitor up to 16 LED boards at once. Each PMT will be powered
593 by a unique low cost power supply developed for the SK UKLI system. These will be housed
594 in a small 2–3 U server rack. The signals from the PMTs will then go to the dedicated HK
595 electronics channels that are set up for monitoring.

596 **9 Control System for LEDs**

597 The LEDs are driven by a differential LVDS signal originating from the FPGA. The FPGA
598 in use is the Genesys 2 [19] development board, which operates a pulsing VHDL module
599 clocked at 300 MHz. Pulses are generated on the rising edge of this clock, and toggling the
600 output (i.e., asserting and then deasserting the trigger) requires a minimum of two clock
601 cycles. Consequently, the shortest achievable pulse duration in this configuration is 3.3 ns.

602 One of the main limitations of this setup is the coarse time resolution: pulse durations
603 are effectively constrained to integer multiples of 3.3 ns. To achieve a broader and more
604 finely resolved spectrum of optical injection into the detector, improved temporal precision
605 is necessary. This is accomplished using the Xilinx IODELAY primitive, originally designed for
606 high-speed interface timing alignment. The IODELAY module permits fine-tuning of signal
607 timing to account for PCB trace mismatches, and in this application, it is repurposed to
608 introduce controlled delays between pulses.

609 To generate shorter pulses, two identical signals are created, one of which is delayed
610 using IODELAY. These signals are then combined using a logical AND operation, producing
611 a narrower pulse. Since the IODELAY module requires one clock cycle to process the input,
612 both signals—regardless of whether they are delayed—must pass through an IODELAY stage
613 to ensure temporal synchronisation.

614 Conversely, to produce longer pulses, the same methodology is applied, but the signals are
615 combined using a logical OR gate instead. This approach extends the pulse width beyond the
616 base clock resolution, enabling pulse durations ranging from approximately 1.5 ns to 4.5 ns
617 in 49 discrete steps. The lower bound is determined by the threshold of the LVDS-to-TTL
618 converter, which does not respond to pulses shorter than approximately 1.5 ns .

619 For channels using the longest optical fibres, this extended range is sufficient, given
620 the intrinsic dispersion in the fibre optics of around 5 ns. However, shorter fibres require
621 additional pulse shaping. To this end, an additional mechanism is implemented using a for
622 loop structure within the FPGA logic. This allows the pulse to persist for multiple clock
623 cycles, effectively producing longer pulses by repetition. However, due to FPGA architecture
624 constraints, each iteration of the loop consumes a clock cycle, necessitating careful timing
625 control. For instance, to produce a 6.6 ns pulse, the loop must be configured for two cycles,
626 accounting for the loop overhead.

627 Further refinement is under investigation through the daisy-chaining of multiple IODELAY
628 modules. This would enable sub-nanosecond granularity by introducing additional interme-
629 diate delay steps. While promising, this technique requires further validation and testing.

630 The pulse control data structure is currently under development. There are two types
631 of pulse description considered. In the first option, the software interface would require two
632 parameters per channel: a *coarse* step and a *fine* step, reflecting the approach used in the SK

633 system. The other option would be just a single variable and then simple logic turning that
634 variable into the *coarse* and *fine* step that the internal logic requires. Two hardware modules
635 are planned: one for generating the single shortest possible pulse (to minimise latency), and
636 another for multi-cycle pulses using programmable duration. A selection logic will assess the
637 input and route it to the appropriate module based on the desired pulse characteristics.

638 Each LED channel will be controlled independently, allowing for unique pulse configura-
639 tions across channels. The global trigger will be derived from the system clock, and each
640 channel will pulse in a predefined sequence while triggered from the global trigger. This
641 architecture also supports simultaneous pulsing of multiple channels. Should asynchronous
642 behaviour be required, additional per-channel delay logic can be implemented. Given the
643 five distinct fibre lengths used in the system, each channel group will also include a config-
644 urable delay offset to compensate for propagation time differences. These group delays will
645 be calibrated and fixed, with the option of fine-tuning individual channels post-deployment
646 if necessary.

647 The FPGA programming remains in active development. Inter-crate communication
648 protocols and synchronisation are currently under integration and testing.

649 10 Crate Electronics

650 10.1 Overview

651 The system specification calls for control of up to 122 LED channels, significantly exceeding
652 the channel counts used in current systems such as Super-Kamiokande or LUX-ZEPLIN,
653 which the previous generation of pulser boards are used for. To manage this complexity, the
654 design prioritises ease of use, maintainability, and straightforward deployment, particularly
655 given that the server racks will accommodate hundreds of optical fibres.

656 To achieve this, a system concept originally developed by ATLAS collaborators (specifi-
657 cally by Ashley Greenal) has been adapted. The original design utilises a Genesys 2 FPGA
658 integrated into a half-width Verotec KM6-2 [20] Eurocard-compatible crate for testing pur-
659 poses. This concept has been extended to a full 19-inch rack width, enabling the integration
660 of up to 36 pulser boards within a single crate.

661 Each FPGA is capable of interfacing with up to 38 pulser boards, thereby maximising
662 the utilisation of available LVDS differential pairs, with an additional pair reserved for the
663 laser trigger signal. This configuration ensures full use of the Genesys 2's I/O capacity while
664 maintaining flexibility for future expansion.

665 The system architecture consists of three primary components: the Blade (Section 10.2),
666 Backplane (Section 10.3) and Eurocard (Section 10.4). This modular approach ensures
667 scalability and facilitates debugging, replacement, and upgrades. It also provides a robust
668 foundation for managing high channel counts while maintaining signal integrity and synchro-
669 nisation across the system.

670 10.2 Blade

671 The Blade is a simple, eight layer board, that has a SEAM-40-06.5-L-10-2-A-K-TR [21]
672 connector which is a direct fit for the Genesys 2's FMC connector. It features a PCIE 16X
673 connector at the edge for connectivity to the Backplane. The PCIE was selected by Ashley
674 Greenal as it is a well documented standard connector and there are a large amount of
675 connectors available that can be bought easily. While PCIE connectors are being used, the
676 PCIE standards for communication are not. This is a very dense PCB with all the differential
677 tracks on it, so buried vias and multiple layers will be used. See Figure 33 for a work in
678 progress version.

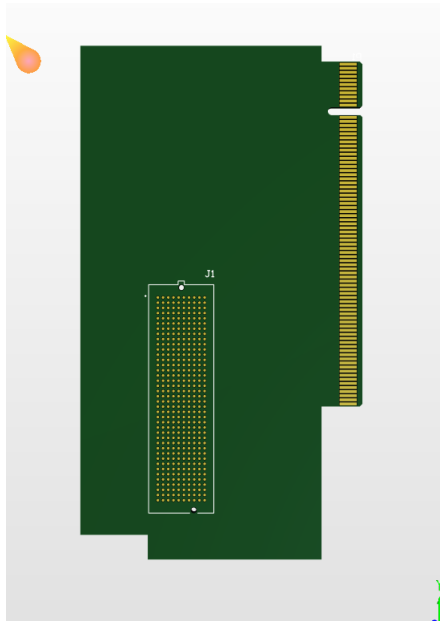


Figure 33: Blade Work in Progress

679 10.3 Backplane

680 The Backplane serves two primary functions: the distribution of differential signals from the
 681 Blade to the Eurocards, and the reception and distribution of power throughout the crate
 682 system. It accepts external power inputs of 12 V and ± 5 V, and includes a basic regulation
 683 circuit to stabilise these supply voltages for downstream use.

684 Given the mechanical constraints and routing complexity, the Backplane is implemented
 685 as a four-layer PCB with impedance-controlled traces to ensure signal integrity across all
 686 differential pairs. It features a single PCIe x16 connector to interface with the Blade, and
 687 three PCIe x8 connectors to interface with the Eurocards.

688 The Eurocards are positioned at slots 2, 8, and 64 within the crate. This arrangement
 689 creates two symmetrical chambers with 48 units spacing between cards, ensuring adequate
 690 space to accommodate the minimum long-term bend radius of the FP400URT optical fibres.
 691 This layout balances mechanical reliability with signal routing efficiency and supports long-
 692 term maintainability of the system. See Figure 34 for a work in progress version.

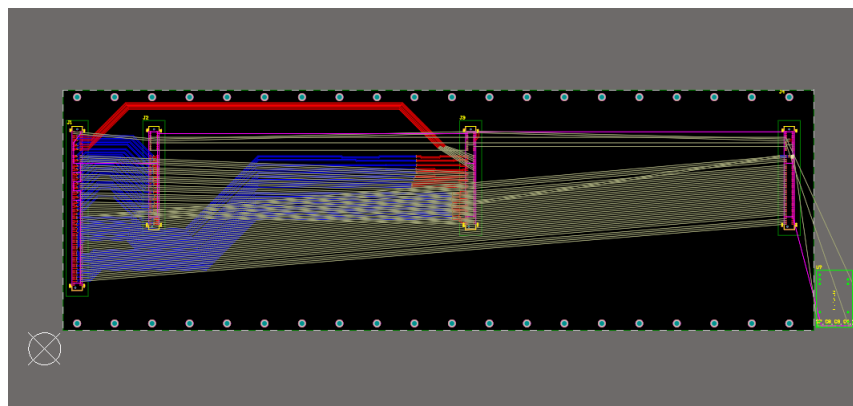


Figure 34: Backplane Work in Progress

693 **10.4 Eurocard**

694 The Eurocard format defines the physical and electrical standard for the crate system, hence
695 the naming convention. Each Eurocard is equipped with a PCIe x8 connector for interfacing
696 with the Backplane, and is designed to host up to 18 pulser boards—nine mounted on each
697 face. Pulser boards connect via FS-1332120 Male[22] connectors, and each socket includes
698 two mounting holes for mechanical standoffs.

699 The board layout on each side consists of two staggered rows: five sockets in the back
700 row and four in the front. The two faces are laterally offset by approximately 10 mm to
701 prevent interference or fibre clashes when the system is fully populated and enclosed within
702 the crate chamber. This offset ensures smooth fibre routing and accommodates the bend
703 radius requirements of FP400URT fibres.

704 Power distribution within each Eurocard is handled by a THD 12-1212 [23]12 V DC-DC
705 regulator. This regulator provides local power isolation for the pulser boards and includes
706 a control pin connected to a PCA9698 [24] 40-pin GPIO expander. This allows for system-
707 level control, enabling or disabling all pulser boards on a card—an essential feature during
708 power-up, especially when the FPGA may inadvertently drive all differential outputs high
709 during reprogramming.

710 The GPIO expander is responsible for enabling the local 12 V regulator and for selectively
711 powering individual pulser boards. This facilitates fault isolation and power savings in
712 channels that are inactive or disconnected. Additional GPIO pins are assigned to monitor
713 output voltage levels via the overcurrent sensing circuitry.

714 To provide per-channel LED power control, an AD5673 [25] DAC is included. It out-
715 puts analogue control voltages to the onboard adjustable regulators on each pulser board,
716 allowing for independent LED drive voltage per channel. Both the GPIO and DAC devices
717 communicate with the system over the I²C protocol.

718 For laser synchronisation, the Eurocard includes a differential-to-NIM conversion stage.
719 This consists of an LVDS-to-TTL converter identical to that used on the pulser boards,
720 followed by a TTL-to-NIM converter. This ensures compatibility with legacy NIM-based
721 timing systems used in external laser triggering. See Figure 35 for a work in progress version.

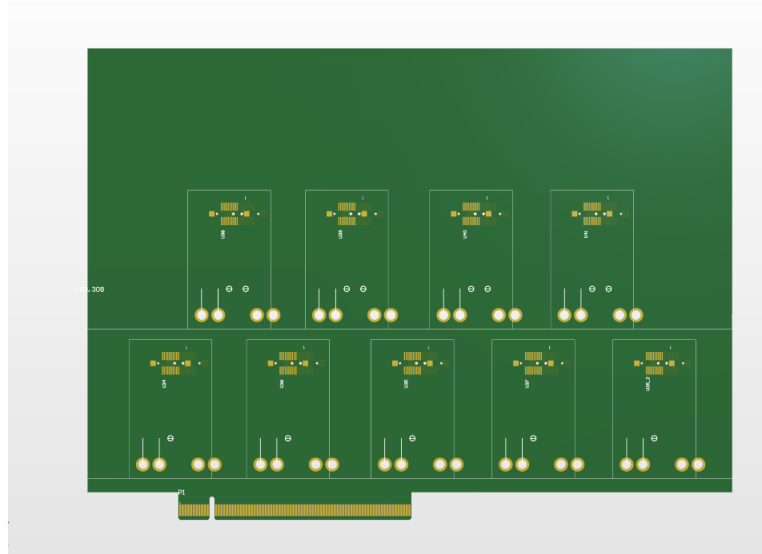


Figure 35: Eurocard Work in Progress

722 11 Conclusions

723 Write this

724 References

- 725 [1] S. Jenkins *et al.*, “HK LI Fibre Specifications,” HK-TN-0091, Aug. 2025.
- 726 [2] Thorlabs. “FP400URT Datasheet.” (2022), [Online]. Available: <https://www.thorlabs.com/drawings/7ade35b092fac3f3-EFB2F350-971A-B4B4-29D36C92039FB538/FP400URT-SpecSheet.pdf> (visited on 07/17/2025).
- 727 [3] Hyper-Kamiokande Outer Detector Group: D. Lodovico, E. Drakopoulou, G. Erofeev,
730 *et al.*, “Outer detector technical report,” HK-TN-0064, 2022.
- 728 [4] H.-K. Collaboration. “WCSim Version 1.12.26.” (2018), [Online]. Available: <https://github.com/WCSim/WCSim/releases/tag/v1.12.26> (visited on 09/16/2025).
- 731 [5] S. Boyd *et al.*, “Hyper-Kamiokande light injector diffuser technical note,” HK-TN-0042,
733 May 2023.
- 735 [6] N. E. M. Association. “NEMA STANDARDS PUBLICATION NO. LI 1-1998.” (1998),
736 [Online]. Available: <https://www.nema.org/docs/default-source/standards-document-library/li1.pdf> (visited on 08/19/2025).
- 738 [7] I. T. AG. “BFR 92P E6327 Datasheet.” (2009), [Online]. Available: https://www.mouser.co.uk/datasheet/2/196/Infineon_LNA_BFR92P_14-73949.pdf (visited on
739 07/17/2025).
- 741 [8] T. I. Incorporated. “LMG1020 Datasheet.” (2018), [Online]. Available: https://www.ti.com/lit/ds/symlink/lmg1020.pdf?ts=1752716909774&ref_url=https%253A%252F%252Fwww.mouser.cn%252F (visited on 07/17/2025).
- 744 [9] E. P. C. Corporation. “EPC2012 Datasheet.” (2012), [Online]. Available: https://www.epc-co.com/epc/Portals/0/epc/documents/datasheets/EPC2012_datasheet.pdf (visited on 07/17/2025).
- 747 [10] E. P. C. Corporation. “EPC8004 Datasheet.” (2023), [Online]. Available: https://www.epc-co.com/epc/Portals/0/epc/documents/datasheets/EPC8004_datasheet.pdf (visited on 07/17/2025).
- 750 [11] Kingbright. “ATS2012UV385 Datasheet.” (2021), [Online]. Available: <https://www.mouser.co.uk/datasheet/2/216/ATS2012UV385-1374632.pdf> (visited on 07/17/2025).
- 752 [12] H. P. K.K. “H10721-210 Datasheet.” (2024), [Online]. Available: https://www.hamamatsu.com/content/dam/hamamatsu-photonics/sites/documents/99_SALES_LIBRARY/etd/H10720_H10721 TPM01062E.pdf (visited on 07/17/2025).
- 755 [13] E. P. C. Corporation. “Design of High Current Nanosecond Resonant Pulse Drivers
756 for Laser Diodes, Lidar, and other Applications.” (2025), [Online]. Available: <https://www.epc-co.com/epc/Portals/0/epc/documents/application-notes/AN032%20Design%20of%20High%20Current%20Nanosecond%20Resonant%20Pulse%20Drivers.pdf> (visited on 07/17/2025).
- 760 [14] L. LED. “ut-67uv365p Datasheet.” (2018), [Online]. Available: <https://www.lc-led.com/products/ut-67uv365p.html> (visited on 08/21/2025).
- 762 [15] T. I. Incorporated. “DS90C402 Datasheet.” (2013), [Online]. Available: <https://www.ti.com/lit/ds/symlink/ds90c402.pdf> (visited on 07/17/2025).

- 764 [16] A. Devices. “LT1963 Datasheet.” (2021), [Online]. Available: <https://www.mouser.co.uk/datasheet/2/609/lt1963a-2256452.pdf> (visited on 07/17/2025).
- 765
- 766 [17] T. I. Incorporated. “LM2347-5 Datasheet.” (2014), [Online]. Available: <https://www.ti.com/lit/ds/symlink/lm2937.pdf> (visited on 07/17/2025).
- 767
- 768 [18] P. Contact. “1331962 Datasheet.” (2025), [Online]. Available: <https://www.phoenixcontact.com/en-us/products/smd-female-connectors-fs-0635-20-fv-r-40-1331962?type=pdf> (visited on 07/17/2025).
- 769
- 770
- 771 [19] Digilent. “Genesys 2 Datasheet.” (2017), [Online]. Available: https://digilent.com/reference/_media/reference/programmable-logic/genesys-2/genesys2_rm.pdf?srsltid=AfmB0orhD9699F1FTC059o719HmCW-0XnE0RnRJf6Thzcvu0vMs-pbAf (visited on 07/17/2025).
- 772
- 773
- 774
- 775 [20] Verotec. “Verotec KM6-2 Datasheet.” (2017), [Online]. Available: <https://www.verotec.co.uk/tech-downloads/Section%201%20-%20KM6-II%20Subracks.pdf> (visited on 07/17/2025).
- 776
- 777
- 778 [21] Samtec. “SEAM-40-06.5-L-10-2-A-K-TR Datasheet.” (2025), [Online]. Available: https://suddendocs.samtec.com/catalog_english/seam.pdf?_gl=1*1soskal*_gcl_au*0DQw0DM2MjE4LjE3NTI3NDg2NTY.*_ga*MTAxNjAxOTQwNS4xNzUyNzQ4NjU2*_ga_3KFNZC07WW*cxE3NTI3NDg2NTUkbzEkZzAkddE3NTI3NDg2NTUkajYwJGwwJGgw (visited on 07/17/2025).
- 779
- 780
- 781
- 782
- 783 [22] P. Contact. “1332120 Datasheet.” (2025), [Online]. Available: <https://www.phoenixcontact.com/en-us/products/smd-male-connectors-fs-0635-20-mv-r-50-1332120?type=pdf> (visited on 08/21/2025).
- 784
- 785
- 786 [23] T. E. AG. “THD 12-1212 Datasheet.” (2025), [Online]. Available: https://www.tracopower.com/sites/default/files/products/datasheets/thd12_datasheet.pdf?t=1752706801 (visited on 07/17/2025).
- 787
- 788
- 789 [24] N. B.V. “PCA9698 Datasheet.” (2010), [Online]. Available: <https://www.nxp.com/docs/en/data-sheet/PCA9698.pdf> (visited on 07/17/2025).
- 790
- 791 [25] A. Devices. “AD5673 Datasheet.” (2020), [Online]. Available: <https://www.analog.com/media/en/technical-documentation/data-sheets/ad5673r-5677r.pdf> (visited on 07/17/2025).
- 792
- 793